JOURNAL OF GEOPHYSICAL RESEARCH, VOL. 104, NO. D12, PAGES 14,321–14,345, JUNE 27, 1999

Uncertainty of measurements of spectral solar UV irradiance

G. Bernhard[1] and G. Seckmeyer

Fraunhofer Institute for Atmospheric Environmental Research, Garmisch-Partenkirchen, Germany

Abstract. Most investigations on the nature and effects of solar ultraviolet (UV) radiation at the Earth's surface require measurements of high accuracy combined with well-defined procedures to assess their quality. Here we present a general evaluation of all relevant errors and uncertainties associated with measurements of spectral global irradiance in the UV. The uncertainties are quantified in terms of dependence of the characteristics of the spectroradiometer, the uncertainty of calibration standards, the solar zenith angle, and atmospheric conditions. The methodologies and equations presented can be applied to most spectroradiometers currently employed for UV research. The sources of error addressed include radiometric calibration, cosine error, spectral resolution, wavelength misalignment, stability, noise, stray light, and timing errors. The practical application of the method is demonstrated by setting up a complete uncertainty table for the mobile spectroradiometer of the Fraunhofer Institute for Atmospheric Environmental Research (IFU). This instrument has successfully participated in several international intercomparisons of UV spectroradiometers. The expanded uncertainty (coverage factor $k = 2$) for measurements of global spectral irradiance conducted with this instrument varies between 6.3% in the UVA and 12.7% at 300 nm and 60° solar zenith angle. The expanded uncertainties in erythemally and DNA weighted irradiances are 6.1% and 6.6%, respectively. These expanded uncertainties are comparable to uncertainties at the 2σ level in conventional statistics. A substantial reduction of these uncertainties would require smaller uncertainties in the irradiance standards used to calibrate the instrument. Though uncertainties caused by wavelength misalignment and noise become prominent in the shortwave UVB, which is the most important spectral range for UV trend detection, the results indicate that the accuracy of the IFU radiometer is sufficient to detect long-term trends in UV arising from a 3% change in atmospheric ozone. The detection of trends caused by a 1% change in ozone may be beyond the capabilities of current instrumentation.

1. Introduction

Solar UV radiation can be detrimental to terrestrial and aquatic ecosystems as well as human health. Because of the decline in stratospheric ozone concentrations observed at high and middle latitudes [*Harris et al.*, 1994], it is expected that UV levels at the Earth's surface will increase. If current and future risks from solar UV radiation are to be quantified, measurements of solar spectral UV irradiance of known quality are an important prerequisite. This paper focuses on the determination of the uncertainty table for measurements of global spectral UV irradiance $E_G(\lambda)$, i.e., the radiant energy dQ arriving per time interval dt, per wavelength interval $d\lambda$, and per area dA on a horizontal surface from all parts of the sky above the horizontal, including the disc of the Sun itself:

$$E_G(\lambda) = \frac{dQ}{dt\, dA\, d\lambda}. \quad (1)$$

$E_G(\lambda)$ is the most commonly used spectral quantity for UV research. However, the measurement of spectral irradiance in the UV is a demanding task [*McKenzie et al.*, 1994]. Difficulties arise mainly from the steep decline of the solar spectrum in the UVB range, which is due to absorption by atmospheric ozone.

The required accuracy of measurements of $E_G(\lambda)$ depends on the intended use of the data. Such uses include, for example, effect studies on biological organisms, providing information to the public about actual UV levels, and investigations on the transfer of radia-

[1]Now at Biospherical Instruments Inc., San Diego, California.

Paper number 1999JD900180.
0148-0227/99/1999JD900180$09.00

tion through the atmosphere and trend detection. For the last point, in particular, high accuracy is required because trends in UV are expected to be small.

The overall uncertainty of a UV measurement depends on the specifications of the instrumentation employed, the uncertainty in the calibration sources, and atmospheric conditions. All points will be addressed thoroughly in this paper. Though very important, the influence of the technical skills of the personnel operating the instruments will not be discussed. All uncertainties reported are consequently based on the assumption that instruments are carefully maintained and characterized. This includes the application of a quality control (QC) plan. In addition, instruments should participate in intercomparison campaigns to assure their quality and to detect systematic errors that would otherwise go undetected. Several such campaigns have been organized in the past in the framework of national, European, and international research programs [e.g., *Gardiner and Kirsch*, 1995; *Webb*, 1997; *Seckmeyer et al.*, 1998; *Thompson et al.*, 1997; *Kjeldstad et al.*, 1997]. These publications also include valuable information on the characterization of instruments and on methods to reduce uncertainties by means of both laboratory investigations and the application of correction procedures.

Several studies in the past have already addressed the problem of how to estimate the uncertainty of spectral UV measurements. Most of these examinations are related to a specific instrument or to radiometry in general. In contrast, this paper (1) is applicable to a great variety of instruments currently deployed worldwide, (2) focuses on the special needs of solar radiometry in the UV range, (3) includes an analysis about the influence of different atmospheric conditions on the determined uncertainties, and (4) gives examples of uncertainties in biologically weighted irradiance derived from spectral measurements. The results are applicable to scanning spectroradiometers that have a spectral bandwidth between 0.3 and 5.0 nm, have a wavelength uncertainty of less than 0.5 nm, use entrance optics with cosine weighting, and are calibrated with tungsten halogen lamps. Most of the spectroradiometers currently used for UV research meet these specifications.

It is worthwhile to give some examples of investigations conducted to estimate the uncertainty of UV measurements. *Bener* [1960] gives a detailed uncertainty report for measurements of a spectroradiometer deployed in the 1950s and 1960s in Davos-Platz, Switzerland. However, since his measurements were carried out at 1590 m above sea level and his equipment was quite different from current instrumentation, his results can only partly be transferred to today's needs.

The instruments that are currently most often used to measure spectral UV irradiance are Brewer ozone spectrophotometers [*Brewer*, 1973; *Bais et al.*, 1996]. A comprehensive characterization and determination of uncertainties are given by *Köhler et al.* [1995]. *McKenzie et al.* [1992] describe the characterization and evaluation of the errors of a spectroradiometer developed in New Zealand.

The above studies are only applicable to the particular instrument under test. In contrast, *Bais* [1997] gives a qualitative overview of the errors and uncertainties involved in the measurement of $E_G(\lambda)$. In the framework of activities of the Scientific Advisory Group (SAG) on UV measurements established by the World Meteorological Organisation (WMO), a document regarding guidelines for site quality control of UV monitoring was published [*Webb et al.*, 1998]. A standard method of estimating uncertainty is proposed, with special emphasis on comparability between different measurement sites. According to *Webb et al.* [1998], the actual uncertainty of a single measurement at a given site may deviate from this standard estimate. In contrast, our investigation focuses on the actual uncertainty of individual instruments.

Recently, a comprehensive textbook on radiometry was published by *Kostkowski* [1997]. As an example, the measurement of direct solar spectral irradiance between 295 and 315 nm is described. Some errors in spectroradiometry are addressed more comprehensively there than can be done here. However, in contrast to *Kostkowski* [1997], we focus on the measurement of global rather than direct irradiance and we also consider the needs of UV effect research and the influence of the atmosphere on uncertainties.

In section 3, all error sources and uncertainties arising in solar UV spectroradiometry are described and quantified in a general way. In section 4, the method is then applied to measurements of the "mobile spectroradiometer" of the Fraunhofer Institute for Atmospheric Environmental Research (IFU), establishing an uncertainty report for this instrument.

2. Material and Methods

2.1. Method to Express Systematic Errors and Uncertainties

In spectoradiometry, the simple equation

$$E_M(\lambda) = \frac{S_M(\lambda)}{r(\lambda)} \tag{2}$$

is frequently used to determine the spectral irradiance $E(\lambda)$ produced by the radiation source to be measured. In (2), $S_M(\lambda)$ is the signal of the radiometer when measuring the source, $r(\lambda)$ is the spectral responsivity of the instrument, and $E_M(\lambda)$ is the measurement result. In practice, the measured irradiance $E_M(\lambda)$ will deviate from the "true" spectral irradiance $E(\lambda)$ owing to systematic and statistical errors. Systematic errors describe the deviation between the "true value" of the quantity to be measured and the average of a large number of measurements of this quantity carried out under repeatable conditions. In contrast, statistical errors express the fluctuation of individual measurements around the average.

2.1.1. Systematic errors. The deviation of the measured irradiance $E_M(\lambda)$ from the true irradiance $E(\lambda)$ due to systematic errors can be expressed by

$$E_M(\lambda) = E(\lambda)\, R(\lambda, x_1, x_2, ...x_n) \tag{3}$$

where the factor $R(\lambda, x_1, x_2, ...x_n)$ takes into account all sources of systematic error affecting the measurement. If the different error sources are independent from each other, which is the case for all errors introduced below unless stated otherwise, $R(\lambda, x_1, x_2, ...x_n)$ can be split into several parts:

$$\begin{aligned} &R(\lambda, x_1, x_2, ...x_n) = \\ &R_{X_1}(\lambda, x_1)\, R_{X_2}(\lambda, x_2) ... R_{X_n}(\lambda, x_n). \end{aligned} \tag{4}$$

The factors $R_{X_i}(\lambda, x_i)$ with $(1 \leq i \leq n)$ represent n different sources of systematic error X_1, X_2, ..., X_n and are defined by

$$R_{X_i}(\lambda, x_i) = \frac{E_{X_i}(\lambda, x_i)}{E(\lambda)} \tag{5}$$

where, again, $E(\lambda)$ is the true spectral irradiance and $E_{X_i}(\lambda, x_i)$ is the idealized irradiance that would be measured if only the error source X_i existed. The variable x_i expresses the parameter that characterizes the source of error X_i. For example, the error source "wavelength shift" explained in section 3.4 and abbreviated by the character W is characterized by the magnitude of the shift $\Delta\lambda$. Thus $R_W(\lambda, \Delta\lambda) = E_W(\lambda, \Delta\lambda)/E(\lambda)$ is the factor by which the measured irradiance $E_M(\lambda)$ deviates from $E(\lambda)$ owing to a wavelength shift of $\Delta\lambda$, neglecting all other systematic errors.

If a systematic error X_i can be completely characterized, the measured irradiance $E_M(\lambda)$ can be corrected for this error simply by multiplying $E_M(\lambda)$ with the correction factor $K_{X_i}(\lambda, x_i) = 1/R_{X_i}(\lambda, x_i)$. In reality, systematic errors can never be completely determined and corrected for, and uncertainties in the measurement result are therefore unavoidable.

2.1.2. Uncertainties. Throughout this paper, the way of expressing uncertainties is in accordance with the International Standards Organization (*ISO*) [1993]. Here uncertainties evaluated by a statistical analysis of a series of observations are denoted "type A standard uncertainites" u_A. Usually, u_A is equal to the sample standard deviation of the mean $\bar{s}$

$$u_A = \bar{s} = \frac{1}{\sqrt{m}}\, s \tag{6}$$

where s is the sample standard deviation derived from m independent measurements of the given quantity. Type A uncertainties can consequently be reduced by increasing the number of measurements.

ISO [1993] denotes uncertainties originating from (incompletely corrected) systematic errors as "type B standard uncertainties." These are determined by means other than by the statistical analysis of a series of measurements. According to *ISO* [1993], the type B standard uncertainty u_B related to a systematic error is

$$u_B = \frac{1}{2\sqrt{3}}(a_+ - a_-) \tag{7}$$

where a_+ is the estimated upper limit and a_- is the estimated lower limit for the quantity being measured. (This definition is based on the assumption that the probability distribution for a measurement result is rectangular; that is, the probability that the true value lies within the interval a_+ and a_- is constant and is zero outside this interval. This is the usual assumption if no information about the actual distribution is available. For details, see *ISO* [1993] and *Kostkowski* [1997]). Type B uncertainties cannot be reduced by increasing the number of measurements.

Following the recommendations of *ISO* [1993], all standard uncertainties of type A, u_{A_j}, and type B, u_{B_i}, are combined in quadrature:

$$u_{\text{comb}} = \sqrt{\sum_j u_{A_j}^2 + \sum_i u_{B_i}^2} \tag{8}$$

Note that (8) is valid only if all uncertainty components are uncorrelated. If this is not the case, a covariance term has to be added to (8); see *ISO* [1993].

The resulting combined uncertainty u_{comb} is finally multiplied by a coverage factor k to derive the expanded uncertainty U of the final measurement result. In this paper, the coverage factor is set as $k = 2$. Thus expanded uncertainties reported herein are comparable to uncertainties on the "2σ level" in conventional statistics.

2.2. Radiative Transfer Model

The studies concerning the dependence of uncertainties on atmospheric conditions are based on model calculations. The model employed is the pseudospherical version of the radiative transfer model UVSPEC [*Dahlback and Stamnes*, 1991; *Mayer et al.*, 1997], which has been shown to agree well with measurements: systematic differences between measurement and model were found to range between −11% and +2% for wavelengths between 295 and 400 nm and solar zenith angles (SZA) up to 80° [*Mayer et al.*, 1997]. The model proved to be accurate enough to be used in this study to determine the effects of solar elevation (position of the Sun in degrees measured from the horizon), total ozone, albedo, and aerosol optical depth on spectral UV.

3. Sources of Systematic Errors and Uncertainties

In the following, the different sources of errors in solar radiometry are compiled in the order of decreasing importance.

3.1. Radiometric Calibration

With the radiometric calibration, the spectral responsivity $r(\lambda)$ of a radiometer is determined

$$r(\lambda) = \frac{S_L(\lambda)}{E_L(\lambda)}. \quad (9)$$

$E_L(\lambda)$ is the irradiance produced by a calibration source, and $S_L(\lambda)$ is the signal of the radiometer when measuring the source. According to (2), the ratio $S_M(\lambda)/r(\lambda)$ is then the measured irradiance $E_M(\lambda)$.

In solar UV radiometry, tungsten halogen lamps are usually used as the calibration source. Reference standards based on these lamps are available from national standards laboratories such as the National Institute of Standards and Technology (NIST) in the United States, the Physikalisch Technische Bundesanstalt (PTB) in Germany, or the National Physical Laboratory (NPL) in Great Britain. Further uncertainties in the determination of the instrument responsivity arise from the aging of the standards between their calibration and use, the conditions during lamp operation, and the characteristics of the spectroradiometer.

3.1.1. Uncertainties in the certificates of reference standards. Table 1 gives an overview of uncertainties in reference standards reported by different standards laboratories. In an intercomparison of spectral irradiance standards organized between 1987 and 1990 by the Consultative Committee on Photometry and Radiometry (CCPR), the irradiance scales of 12 national standards laboratories were compared [*Walker et al.*, 1991]. The double standard deviation (2σ) of the measurements of all groups was about 4% in the UV. This equals or exceeds the expanded uncertainties given in Table 1.

Table 1. Expanded Uncertainties (Coverage Factor $k = 2$) of Reference Standards From Different Standards Laboratories According to Calibration Certificates

Wavelength, nm	Uncertainty, %
National Institute of Standards and Technology, United States	
Lamp Type: FEL 1000 W, T6, Osram-Sylvania	
250	± 1.82
350	± 1.09
654.6	± 0.91
Physikalisch Technische Bundesanstalt, Germany	
Lamp Type: FEL 1000 W, General Electric	
270 - 400	± 3
400 - 800	± 1.6
Physikalisch Technische Bundesanstalt, Germany	
Lamp Type: FEL 1000 W, T6, Osram-Sylvania	
280 - 300	± 1.5
300 - 400	± 1.0
400 - 700	± 0.8
National Physical Laboratory, England	
Lamp Type: M28, 100 W	
280	± 4.0
350	± 2.5
400 - 695	± 1.5

In order to investigate the differences of standard lamps, we have compared seven reference standards of type FEL calibrated by PTB. For none of these lamps did the burn time exceed 10 hours after calibration at PTB. Three of these lamps were fabricated by General Electric, and their calibration refers to the old pyrometer-based spectral irradiance scale of PTB, which was used until 1995 [*Sperfeld et al.*, 1996]. Four lamps were of the newer T6 type made by Osram-Sylvania. Their calibration refers to the new detector-based PTB scale [*Sperfeld et al.*, 1996]. All lamps were compared in the IFU calibration laboratory using the IFU spectroradiometer. For details, see *Bernhard* [1997]. For wavelengths between 280 and 700 nm, we found the calibration of the new T6 type lamps to be in agreement with each other, to within ±0.3%. This is within the uncertainties given by PTB; see Table 1. In the wavelength range 530-700 nm, the irradiance scales of the old and new types were found to agree on the ±0.5% level. However, at 325 nm, both types disagreed with each other by 4%, which is at the very limit of PTB's uncertainty estimate. A further test with an M28 type lamp calibrated by NPL showed a discrepancy of more than 6% at 300 nm compared with the new PTB scale. These deviations indicate that the uncertainties of lamps disseminated by standards laboratories may be larger than specified. From our findings we conclude that 3.5% is a reasonable estimate for the expanded standard uncertainty ($k = 2$) of current reference standards in the UV. However, this estimate is itself subject to uncertainties because our survey is based on nine lamps only.

3.1.2. Aging of standard lamps. The irradiance produced by standard lamps changes with burn time. According to PTB, the drift of FEL lamps from General Electric is 0.03%/hour in the visible range and 0.05%/hour at 300 nm [*Sperling et al.*, 1996]. Moreover, sudden changes (jumps) of up to 1% in the radiation output of these lamps may occur at unpredictable intervals. NIST seasons FEL lamps for 40 hours and only lamps that then exhibit a change at 654.6 nm of less than 0.5% in 24 hours (= 0.02%/h) after this burn-in period are used for reference standards [*Walker et al.*, 1987]. PTB reports that the continuous drift of the new FEL lamps from Osram-Sylvania is less than ±0.01%/hour at 300 nm [*Sperling et al.*, 1996]. However, we have seen jumps of about 0.5% with these new Osram-Sylvania FEL lamps. For both FEL lamp types, it is therefore advisable to have at least three standards at place that are regularly compared.

In addition to the deterioration of FEL standards, we have studied the drift of 100 W lamps of type M28 and of type Halostar from Osram, which are used at

IFU as working standards. In the visible the deterioration of five lamps was measured with a luxmeter of PRC Krochmann by continously monitoring their illuminance over a period of up to 160 hours. The drift in the UV was determined with the IFU spectroradiometer and control lamps, which were only shortly in use for comparison with the test lamps. After a burn-in time of about 10 hours, the lamp irradiance usually decreases by about 0.02%/hour in the visible and by about 0.04%/hour to 0.08%/hour at 300 nm. Although these drifts are somewhat larger than the drifts of FEL lamps, the lamps deteriorate in a very predictable (and thus correctable) manner and exhibit no jumps.

3.1.3. Operation of standard lamps. The lamp current is the most critical parameter. According to *Webb et al.* [1994] and *Sperling et al.* [1996], a 1% change in lamp current leads to a 10% change in $E_L(\lambda)$ at 300 nm. More generally, *Kostkowski* [1997] states that the percentage change in the spectral irradiance of FEL lamps is approximately $5 \times (600/\lambda)$ times the percentage change in current, where λ is the wavelength in nanometers. To check whether this relation is also applicable for our 100 W lamps, we operated a lamp at 8.5 A (nominal current) and 8.4 A (1.2% below nominal current). The difference in the irradiance was 10% at 300 nm and 5.5% at 600 nm, which agrees well with the formula proposed by *Kostkowski* [1997]. Intercomparison campaigns have uncovered significant systematic errors in solar UV measurements due to inaccurate ammeters [*Gardiner and Kirsch*, 1995]. An uncertainty in lamp current of less than 0.01% is desirable, and this can only be achieved with a high-accuracy current source.

The second most important parameter is the distance between the lamp and the reference plane of the radiometer's entrance optics, measured along the optical axis (x axis). NIST certificates specify irradiance values at 500 mm. At this distance the lamp can be regarded as a point source and therefore $E_L(\lambda)$ changes with distance according to the inverse square law: a 1 mm error in distance results in a 0.4% error in irradiance. For PTB standards, which are calibrated at 700 mm, the respective error is reduced slightly to 0.3%.

Sperling et al. [1996] investigated the effect of further alignment errors for FEL lamps. For positioning errors of less than ± 1 mm in the y and z directions (= symmetry axis of the lamp), rotations of less than 0.1° around the y and z axis, and rotations of less than 2° around the x axis, the standard uncertainty in the irradiance is 0.1%. This accuracy can be achieved only by laser alignment (for details, see *Sperling et al.* [1996] and *Kostkowski* [1997]). Alignment errors concerning the entrance optics lead to an additional irradiance uncertainty of 0.1%.

Another source of uncertainty is stray light. This is radiation that is reflected or scattered from the walls of the calibration room or from the table. Stray light must be suppressed as far as possible, e.g., by baffles and black cloths. Methods to determine uncertainties due to stray light are described by *Kostkowski* [1997]. Further sources of error resulting from the method of lamp operation (e.g., the temperature in the laboratory, vibration, ventilation, change of polarity of the lamp, and a too short lamp warm-up time) are addressed by *Webb et al.* [1994], *Sperling et al.* [1996], and *Kostkowski* [1997].

3.1.4. Influence of the radiometer on the irradiance calibration. The geometry of the radiometer's entrance optics may lead to several further calibration uncertainties. For example, if a translucent quartz plate is used to protect the optics, the optical path of the incident radiation is reduced by refraction: a quartz plate (refraction index 1.5) with a thickness of 2.5 mm reduces the optical path by 2.5 mm − (2.5 mm/1.5) = 0.8 mm, which in turn introduces an irradiance error of 0.3% for a calibration distance of 50 cm. The error value may change if a dome rather than a plate is used for protection, because the spherical geometry of the dome prevents a rectilinear propagation of the incident radiation and multiple reflections between diffuser and dome may occur. A method to calculate the reference plane for nonplanar diffusers is described by *Bernhard and Seckmeyer* [1997].

The irradiance produced by a calibration lamp refers to the average irradiance on a receiver with an area specified in the lamp's certificate. For example, PTB specifies an area of 20 mm × 10 mm. Since the radiation field of a FEL lamp is not perfectly isotropic [*Sperling et al.*, 1996], further errors occur if the actual area of the entrance optics deviates from that specified. On the basis of *Sperling et al.* [1996], we have estimated this standard uncertainty to be about 0.1% for entrance optics smaller than 20 mm × 10 mm.

The degree of polarization for FEL lamps is about 3% [*Kostkowski*, 1997]. This introduces a further uncertainty if entrance optics do not depolarize completely.

3.1.5. Interpolation of calibration values. Standards laboratories only provide calibration points in steps of 5 to 20 nm. Because of the curvature in the lamp's spectrum, which is similar to the spectrum of blackbody radiation, linear interpolation may lead to errors of up 4%. NIST recommends the following equation to calculate irradiance values between the calibration points given in a certificate [*Walker et al.*, 1987]:

$$E_L(\lambda) = [A_0 + A_1\lambda + \ldots + A_n\lambda^n]\,\lambda^{-5}\,\exp(a + b/\lambda), \quad (10)$$

where a, b, A_0, A_1, ... A_n are fit parameters. Spectral irradiance values predicted using (10) have an uncertainty of 0.5%. We prefer an interpolation based on cubic splines. In detail, the logarithm of the given calibration points is calculated, the result is interpolated to the required wavelength steps using natural cubic splines, and finally the antilogarithm is applied. Thus the interpolation is based on values ranging within 1 order of magnitude, which leads to smaller interpolation

error than the interpolation without forming the logarithm. To estimate the standard uncertainty of this method, we started with a blackbody function similar to an actual lamp spectrum, selected points at the same wavelengths as given in certificates of PTB (i.e., between 250 and 300 nm points are given in 10 nm steps and in 20 nm steps afterward), performed the interpolation, and finally compared the result with the original blackbody function. Except for the region between the first and second calibration point (i.e., the range between 250 and 260 nm, which is irrelevant for solar measurements), original and interpolated values lay within ±0.1%. This uncertainty estimate is only valid, however, if lamps have no absorption or emission lines, which is not necessarily true for FEL lamps [*Kostkowski*, 1997].

3.2. Cosine Error

The signal of a radiometer for measuring irradiance should be proportional to the cosine of the angle ϑ between the direction of the incident radiation and the normal of the radiometer's entrance optics. The deviation from this ideal response is called cosine error. The ratio $R_C(\lambda)$ of the irradiance measured with a radiometer, which is affected by the cosine error, to the true irradiance is

$$R_C(\lambda) = \frac{\int_{(2\pi)} L(\lambda,\vartheta,\varphi)\, C(\lambda,\vartheta,\varphi)\, \sin(\vartheta)\, d\vartheta\, d\varphi}{\int_{(2\pi)} L(\lambda,\vartheta,\varphi)\, \cos(\vartheta)\, \sin(\vartheta)\, d\vartheta\, d\varphi}, \tag{11}$$

where φ is the azimuth angle of the incident radiation, $L(\lambda,\varphi,\vartheta)$ is the spectral radiance at the radiometer's entrance optics, and $C(\lambda,\vartheta,\varphi)$ is the angular response of the entrance optics, normalized to 1 at $\vartheta = 0°$. Ideally, $C(\lambda,\vartheta,\varphi)$ should be equal to $\cos(\vartheta)$.

When global spectral irradiance $E_G(\lambda)$ is the measurand, (11) can be split in two parts, separating the contributions from the direct Sun and the diffuse (i.e., scattered) sky radiation [*Seckmeyer and Bernhard*, 1993; *Gröbner et al.*, 1996; *Bais et al.*, 1998]:

$$R_C(\lambda) = q(\lambda)\, \frac{C(\lambda,\vartheta_{\mathrm{Sun}},\varphi_{\mathrm{Sun}})}{\cos(\vartheta_{\mathrm{Sun}})} + [1-q(\lambda)]\, D(\lambda), \tag{12}$$

where the angles ϑ_{Sun} and φ_{Sun} are solar zenith and azimuth angle, respectively, and $q(\lambda)$ is the ratio between direct irradiance $E_D(\lambda)$ and global irradiance $E_G(\lambda)$. ($E_D(\lambda)$ is the irradiance produced by unscattered radiation on a horizontal surface. The difference between global and direct irradiance is denoted sky irradiance $E_S(\lambda)$: $E_S(\lambda) = E_G(\lambda) - E_D(\lambda)$).

$D(\lambda)$ is the ratio of the sky irradiance measured with a radiometer that has a cosine error to the true sky irradiance $E_S(\lambda)$. $D(\lambda)$ is calculated with (11), where the integration range excludes the solid angle of the Sun.

UV measurements can be corrected for the cosine error by multiplying the measurement result with the correction factor $K_C(\lambda) = 1/R_C(\lambda)$. Because of the uncertainties in $q(\lambda)$, $C(\lambda,\vartheta_{\mathrm{Sun}},\varphi_{\mathrm{Sun}})$, and $D(\lambda)$, the accuracy of the correction is limited. The standard uncertainty $u_{R_C}(\lambda)$ of $R_C(\lambda)$ is expressed by

$$\begin{aligned} u_{R_C}(\lambda) &= \left[\left(\tfrac{\partial R_C}{\partial q}u_q\right)^2 + \left(\tfrac{\partial R_C}{\partial C}u_C\right)^2 + \left(\tfrac{\partial R_C}{\partial D}u_D\right)^2\right]^{0.5} \\ &= \left\{\left[\frac{C(\lambda,\vartheta_{\mathrm{Sun}},\varphi_{\mathrm{Sun}})}{\cos(\vartheta_{\mathrm{Sun}})} - D(\lambda)\right]^2 u_q^2 \right. \\ &\quad + \left[\frac{q(\lambda)}{\cos(\vartheta_{\mathrm{Sun}})}\right]^2 u_C^2 \\ &\quad \left. + [1-q(\lambda)]^2\, u_D^2\right\}^{0.5}, \end{aligned} \tag{13}$$

where u_q, u_C and u_D are the standard uncertainties of $q(\lambda)$, $C(\lambda,\vartheta_{\mathrm{Sun}},\varphi_{\mathrm{Sun}})$, and $D(\lambda)$, respectively. The magnitudes of these uncertainties depend very much on the instrument specifications and the prevailing atmospheric conditions, as discussed below.

3.2.1. Range and uncertainty of $C(\lambda,\vartheta,\varphi)$. Many UV spectroradiometers currently deployed exhibit deviations from the ideal cosine of more than 10% at $\vartheta = 60°$. For larger ϑ the deviation may be even greater [e.g., *Gardiner and Kirsch*, 1995; *Webb et al.*, 1994; *Webb*, 1997; *Seckmeyer et al.*, 1998]. Therefore the cosine error is one of the most important sources of error in solar spectroradiometry. However, entrance optics with smaller cosine errors are now available [*Bernhard and Seckmeyer*, 1997; *Bais*, 1998].

The cosine error may also depend significantly on wavelength and azimuth angle and, additionally, can change with time. For example, instruments that have an integrating sphere may have a pronounced azimuthal dependence [*McKenzie et al.*, 1993; *Webb*, 1997] and the coating of the sphere may age. This complicates the application of correction algorithms.

$C(\lambda,\vartheta,\varphi)$ may also depend on the polarization of the incident radiation. Since sky radiance and the radiation of an FEL lamp are polarized, further uncertainties have to be considered. To estimate their magnitude, measurements of the radiance distribution of sky radiation on dependence of polarization are required. Although this is possible [*Coulson*, 1988; *Liu and Voss*, 1997; *Voss and Liu*, 1997], these measurements are rather elaborate and are probably too time-consuming to be performed within a spectrum of global irradiance. A more satisfactory solution is to choose entrance optics with low dependence on polarization.

The usual method to determine $C(\lambda,\vartheta,\varphi)$ is to mount the radiometer on a turn table with its axis going through the center of the reference plane of the radiometer's entrance optics. The radiometer then measures the irradiance of a fixed lamp as a function of ϑ, φ, and λ. To reduce uncertainties in the determination

of $C(\lambda, \vartheta, \varphi)$, the integration time of the radiometer must be sufficiently long. For details, see *Seckmeyer and Bernhard* [1993], *Kostkowski* [1997], *Feister et al.* [1997], and *Webb et al.* [1994].

Uncertainties in the determination of $C(\lambda, \vartheta, \varphi)$ arise mainly from misalignment. For example, if the zero position of the turntable is wrong by 1°, $C(\lambda, \vartheta, \varphi)$ is in error by 3% at $\vartheta = 60°$ and by about 20% at $\vartheta = 85°$. The standard uncertainty of the zero position of our facility to measure the angular response of entrance optics is 0.08°; the uncertainty in positioning the center of the entrance optics above the resolving axis is 0.8 mm in both relevant directions. These uncertainties in alignment lead to a standard uncertainty ($k = 1$) in $C(\lambda, \vartheta, \varphi)$ of 1.1% at $\vartheta = 60°$ and 2.8% at 80°.

3.2.2. Range and uncertainty of $q(\lambda)$. The ratio $q(\lambda) = E_D(\lambda)/E_G(\lambda)$ depends on all the parameters that affect UV radiation at the Earth's surface. The ideal method to determine $q(\lambda)$ is to measure $E_D(\lambda)$ and $E_G(\lambda)$ simultaneously with two independent spectroradiometers. If $E_D(\lambda)$ and $E_G(\lambda)$ are measured alternately with one instrument, a time-interpolation is necessary, and changing atmospheric conditions (e.g., moving clouds) lead to higher uncertainties compared to the simultaneous schedule.

The ratio $q(\lambda)$ can also be approximated by a radiative transfer model, as suggested by *McKenzie et al.* [1992] and *Seckmeyer and Bernhard* [1993]. We have recalculated this ratio with the more accurate UVSPEC model introduced in section 2.2 for a variety of SZAs and three different aerosol optical depths $\tau(\lambda)$. The results are shown in Figure 1. Further input parameters of the model were: total ozone 320 Dobson units (DU), Ångström's turbidity parameter $\alpha = 1$, surface albedo = 0.05, altitude = 730 m. Clearly, the ratios depend on solar zenith angle and aerosol properties, and these parameters are therefore necessary for a meaningful estimate of $q(\lambda)$. Fortunately, $q(\lambda)$ depends only slightly on total ozone [*Zeng et al.*, 1994].

For overcast conditions, when the Sun is always hidden, $q(\lambda)$ is effectively zero resulting in $R_G(\lambda) = D(\lambda)$. For broken cloud situations the application of current one-dimensional models is not appropriate and simultaneous measurements of $E_D(\lambda)$ and $E_G(\lambda)$ may be necessary.

Feister et al. [1997] use global and diffuse irradiance measurements of two broadband UVB sensors to determine $q(\lambda)$ and, based on that, correct measurements of a Brewer spectrophotometer for the cosine error. The advantage of this method is that diffuse and global data are available simultaneously without the need of operating two expensive spectroradiometers. *Feister et al.* [1997] include a comprehensive uncertainty estimate of the method and a parameterization of $q(\lambda)$ as a function of λ, ϑ_{Sun}, and $\tau(350\text{ nm})$.

3.2.3. Range and uncertainty of $D(\lambda)$. To estimate the diffuse ratio $D(\lambda)$, it is often assumed that the sky radiance $L(\lambda, \vartheta, \varphi)$ is isotropic; that is,

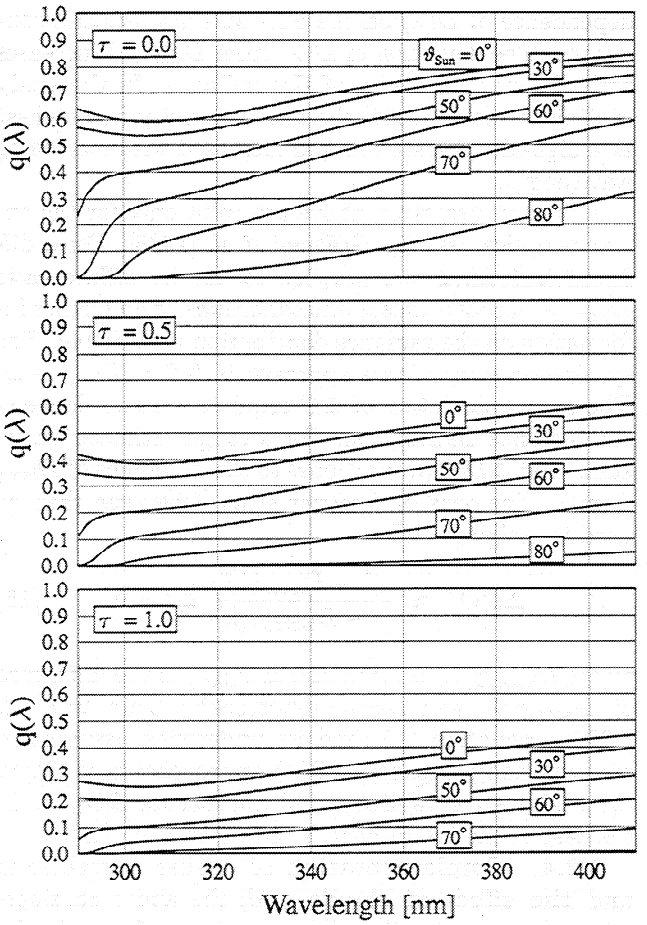

Figure 1. Ratio $q(\lambda)$ between direct and global spectral irradiance in dependence of wavelengths for different zenith angles ϑ_{Sun} and aerosol optical depths $\tau(\lambda)$. The values are based on UVSPEC model calculations assuming a total ozone column of 320 Dobson units (DU). Aerosol optical depths at 300 nm are (top) $\tau(300\text{ nm}) = 0.0$; (middle) $\tau(300\text{ nm}) = 0.5$; and (bottom) $\tau(300\text{ nm}) = 1.0$.

$L(\lambda, \vartheta, \varphi)$ does not depend on ϑ and φ. In this case, $D(\lambda)$ simplifies to

$$D_{\text{isotr}}(\lambda) = 2\int_0^{\pi/2} C(\lambda, \vartheta, \varphi)\, \sin(\vartheta)\, d\vartheta. \qquad (14)$$

Gröbner et al. [1996] have investigated the deviation of $D_{\text{isotr}}(\lambda)$ from the true factor $D(\lambda)$ for cloudless skies by measuring sky radiance $L(\lambda, \vartheta, \varphi)$ in addition to their global measurements of $E_G(\lambda)$. The study takes into account cloudless sky situations for varying atmospheric and geographic conditions (SZA between 10° and 80° and aerosol optical depths at 320 nm between 0.03 and 0.6). For their instrument, $D_{\text{isotr}}(\lambda)$ is 0.883; that is, irradiance produced by isotropic sky radiance is underestimated by 11.7%. The true factor $D(\lambda)$ derived from the radiance measurements is 0.833 ± 0.03 at 310 nm, 0.880 ± 0.03 at 320 nm, 0.870 ± 0.035 at 350 nm, and 0.86 ± 0.05 at 400 nm. The plus/minus ranges of $D(\lambda)$ are maximum variations caused by the

dependence of $D(\lambda)$ on the SZA and atmospheric conditions. The deviation of $D(\lambda)$ from $D_{\text{isotr}}(\lambda)$ increases with the inhomogeneity of sky radiance. In the study of *Gröbner et al.* [1996] the inhomogeneity was highest at a high-altitude station and increased with increasing wavelength.

All the values given above are valid only for the entrance optics used by *Gröbner et al.* [1996]. For a different instrument we propose to use its diffuse ratio $D_{\text{isotr}}(\lambda)$ for all atmospheric conditions, if no further information on the radiance distribution is available. The systematic error of this approach is $\Delta D = D_{\text{isotr}} - D$. The exact calculation of ΔD requires the knowledge of the radiance distribution. For a rough estimate we assume that ΔD is proportional to the difference of D_{isotr} from 1. The data of *Gröbner et al.* [1996] can then be used to estimate ΔD:

$$\Delta D(\lambda) \approx \frac{|1 - D_{\text{isotr}}(\lambda)|}{|1 - D_{\text{isotr},G}(\lambda)|} \Delta D_G(\lambda) \qquad (15)$$

where $D_{\text{isotr},G}(\lambda)$ is 0.833 and $\Delta D_G(\lambda)$ is the difference of $D_{\text{isotr},G}(\lambda)$ and $D_G(\lambda)$ reported by *Gröbner et al.* [1996]. Equation (15) and its underlying assumption are reasonable because $\Delta D(\lambda)$ approaches zero, when the cosine error vanishes, and approaches $\Delta D_G(\lambda)$ in the case of the instrument by *Gröbner et al.* [1996].

3.2.4. Implementation of cosine corrections and the effect of clouds. All the above considerations refer to cloudless sky situations. To study the effect of clouds, *Bernhard and Seckmeyer* [1997] have carried out measurements with two almost identical spectroradiometers. One was equipped with a diffuser, which had a relatively high cosine error ($D_{\text{isotr}}(\lambda) = 0.903$), and the second instrument used newly developed entrance optics with low cosine error ($D_{\text{isotr}}(\lambda) = 0.981$). For a day with cloudless sky the difference between the uncorrected measurements of both instruments was up to 12%. This difference was explained by the cosine error, and, consequently, correction factors $K_C(\lambda) = 1/R_C(\lambda)$ were applied to the measurements. These were calculated with (12), where $q(\lambda)$ was derived from a model and $D(\lambda)$ was approximated by $D_{\text{isotr}}(\lambda)$. For a day with cloudless sky, $K_C(350\text{ nm})$ of the instrument with the diffuser varied between 1.073 and 1.134, depending on the SZA. $K_C(350\text{ nm})$ for the second instrument was between 1.00 and 1.04. After the correction the results of both instruments agreed to within 2% at 350 nm. This good agreement gives confidence in the way the correction factors were calculated for the particular cloudless day chosen by *Bernhard and Seckmeyer* [1997].

Bernhard and Seckmeyer [1997] set $q(\lambda) = 0$ for overcast situations, and assumed that the sky radiance is isotropic. Again, the difference in the results of both instruments can be explained. This indicates that the assumption of isotropic sky radiance is valid, although it can be expected that under homogenous clouds, zenith radiance is likely to be greater than that originating near the horizon [*Grant and Heisler*, 1997].

For the day with broken cloud chosen by *Bernhard and Seckmeyer* [1997], the ratio of the uncorrected measurements of both instruments alternates between the ratio for clear sky and overcast sky, in dependence of whether the Sun is visible or not. If no information about Sun visibility exists, we suggest setting $K_C^{\text{cloudy}} = 1/2(K_C^{\text{clear}} + K_C^{\text{overcast}})$, where K_C^{cloudy}, $K_C^{\text{clear}}(\lambda)$, and $K_C^{\text{overcast}}(\lambda)$ are the correction factors for broken cloud, clear-sky, and overcast situations (i.e., $q(\lambda) = 0$), respectively. We propose to set the uncertainty $u_{K_C}^{\text{cloudy}}$ of K_C^{cloudy} as follows:

$$u_{K_C}^{\text{cloudy}} = u_{K_C}^{\text{clear}} + \frac{1}{2\sqrt{3}} |K_C^{\text{clear}}(\lambda) - K_C^{\text{overcast}}(\lambda)|, \qquad (16)$$

where $u_{K_C}^{\text{clear}}$ is the uncertainty of the correction factor for cloudless sky, calculated with (13). The second term in (16) describes the additional uncertainty introduced by cloud variability; its formulation is based on (7). Since it cannot be expected that both terms in (16) are independent, they are added rather than combined in quadrature. As a consequence of the underlying data set, which does not allow appropriate statistics, the proposed method to estimate $u_{K_C}^{\text{cloudy}}$ is itself the subject of considerable uncertainties and may therefore not be appropriate for all conceiveable cloud situations.

3.3. Spectral Resolution

The entrance and exit apertures of a monochromator have finite widths. As a consequence, not only do photons with the desired wavelength λ_0 pass through the monochromator but also those with wavelengths inside a certain interval around λ_0. When the monochromator is set to a fixed wavelength λ_0, its transmittance as a function of wavelength is called the slit function $f(\lambda)$. The width of the slit function is usually quantified by the full width of the function at half of its maximum (FWHM) and is denoted the bandwidth B of the monochromator. In practice, the slit function is usually determined by scanning a monochromatic radiation source (e.g., a selected line from a low-pressure Mercury lamp or a laser) by the spectroradiometer. Neglecting changes in the spectral responsivity over the scanning range, the slit function is the mirror image of the recorded spectrum with the mirror plane at the wavelength of the incident radiation.

Typical bandwidths of current UV spectroradiometers are between 0.3 and 2.0 nm FWHM [*Webb*, 1997]. Since most Fraunhofer lines of the solar spectrum are narrower than 0.01 nm (see Figure 2), the Fraunhofer structure is smoothed out considerably by these instruments. The measured irradiance $E_R(\lambda, f)$ is the true irradiance $E(\lambda)$ convolved with the instrument's slit function $f(\lambda)$:

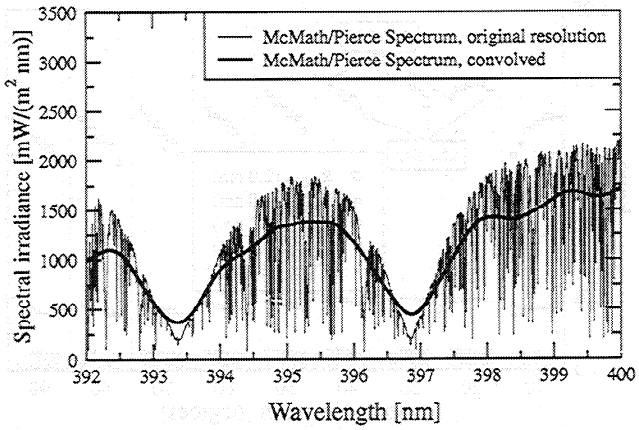

Figure 2. High-resolution solar spectrum in the region of the calcium doublet obtained with the Fourier transform spectrometer at the McMath/Pierce Solar Telescope situated on Kitt Peak, Arizona. The thin line represents the spectrum in original resolution, while the thick line denotes the spectrum convolved with the slit function of the mobile Fraunhofer Institute for Atmospheric Environmental Research (IFU) spectroradiometer of 0.574 nm full width at half maximum (FWHM).

$$E_R(\lambda, f) = \frac{\int E(\lambda')\, f(\lambda - \lambda')\, d\lambda'}{\int f(\lambda')\, d\lambda'} \qquad (17)$$

In the example of Figure 2 a high-resolution solar spectrum is compared with the same spectrum convolved with the slit function of the mobile IFU spectroradiometer, which has a FWHM of 0.574 nm, thus mimicking a spectral measurement of the IFU instrument. The high-resolution spectrum was obtained with the Fourier transform spectrometer at the McMath/Pierce Solar Telescope situated on Kitt Peak, Arizona [*Kurucz et al.*, 1984]. The resolution of this instrument is about 0.01 cm^{-1} in the UV, corresponding to 0.00012 nm at 350 nm. Since most Fraunhofer lines are broader than 0.001 nm [*Moore*, 1966], the reproduction of the Fraunhofer structure is hardly influenced by the resolution of the Kitt Peak spectrum.

The ratio of both data sets in Figure 2 reaches values of up to 14. There is some controversy as to whether this deviation should be regarded as an error or whether it is better denoted as an instrumental feature: it has to be named an error if the quantity to be measured is global spectral irradiance $E_G(\lambda)$ as defined in (1). Obviously, the problem disappears if the measurand is "spectral irradiance referred to the instrument's slit function." The more suitable definition of the measurand depends on the application of the data. For example, for a meaningful comparison of measured spectra with a model it is advisable to convolve the model results with the instrument's slit function before forming the ratio of both spectra [*Mayer et al.*, 1997]. The comparision is then free from the influence of the instrument's resolution. If measurements of instruments with different resolution are intercompared it may also be useful to normalize their results to a common resolution by means of deconvolution techniques [*Slaper et al.*, 1995]. On the other hand, if the measured data are used to calculate values of biologically weighted irradiance (e.g., erythemal irradiance), the resolution is no longer negligible. For example, owing to the strong decline of the solar spectrum in the UVB, the bandwidth causes a systematic overestimate of spectral irradiance, leading to results of biologically weighted irradiance that are too high. This will be quantified in the following.

3.3.1. Errors in measurements of biologically weighted irradiance due to the resolution of the spectroradiometer. These errors are quantified with the factors $R_{R,\mathrm{Bio}}(B)$, which are defined as the ratio of biologically weighted irradiance determined from measurements of a spectroradiometer with a slit function $f(\lambda)$ to the respective values from an ideal instrument with an infinitesimal bandwidth:

$$R_{R,\mathrm{Bio}}(B) = \frac{\int_0^\infty E_R(\lambda, f)\, A_{\mathrm{Bio}}(\lambda)\, d\lambda}{\int_0^\infty E(\lambda)\, A_{\mathrm{Bio}}(\lambda)\, d\lambda}, \qquad (18)$$

where $A_{\mathrm{Bio}}(\lambda)$ is the relevant biological action spectrum and B is the FWHM of the slit function $f(\lambda)$. Two action spectra were considered. One is the Commission Internationale de l'Éclairage (CIE) action spectrum for erythema $A_{\mathrm{Ery}}(\lambda)$ [*McKinlay and Diffey*, 1987]; the second is the action spectrum of DNA damage $A_{\mathrm{DNA}}(\lambda)$ [*Setlow*, 1974], parameterized according to *Bernhard et al.* [1997]:

$$A_{\mathrm{DNA}}(\lambda) = \begin{cases} \frac{1}{0.0326} \exp\left[13.82\left(\frac{1}{1+\exp[(\lambda\,[\mathrm{nm}]-310)/9]}-1\right)\right], & \lambda \le 370\ \mathrm{nm} \\ 0, & \lambda > 370\ \mathrm{nm} \end{cases} \qquad (19)$$

The ratio $R_{R,\mathrm{Bio}}(B)$ depends not only on bandwidth B but also on the spectral shape of the underlying solar spectrum $E(\lambda)$. With model sensitivity studies based on the UVSPEC model we have confirmed that from all parameters determining biologically weighted irradiance at the ground, mainly solar elevation and total ozone column affect $R_{R,\mathrm{Bio}}(B)$. The variation of $R_{R,\mathrm{Bio}}(B)$ introduced by changes of surface albedo between 0 and 1, aerosol optical depth $\tau(320\ \mathrm{nm})$ between 0 and 1.8, and altitude between 0 and 3000 m is about a factor of 15 smaller than the variation introduced by solar elevation and ozone. Also, the influence of thin clouds is negligible. However, the attenuation of spectral irradiance by convective clouds with high optical density (e.g., thunderstorm clouds) is significantly enhanced in the UVB relative to the UVA [*Mayer et al.*, 1998], which leads to changes of $R_{R,\mathrm{Bio}}(B)$ as well.

To quantify the influence of solar elevation and total ozone on $R_{R,\mathrm{Bio}}(B)$, model spectra were calculated for solar elevations between 0° and 90° and ozone values

between 250 and 400 DU. From the modeled irradiance $E(\lambda)$, $E_R(\lambda, f)$ was calculated for triangular slit functions with bandwidths ranging from 0.3 to 5.0 nm FWHM. Finally, the factors $R_{R,\mathrm{Bio}}(B)$ were calculated for the DNA and erythema action spectra. The DNA weighted ratios $R_{R,\mathrm{DNA}}(B)$ are shown in Figure 3 as a function of solar elevation and ozone column. For the slit function of bandwidth 2 nm, $R_{R,\mathrm{DNA}}(2\,\mathrm{nm})$ varies between 1.028 and 1.040. The respective values for the erythemal weighting range between 1.007 and 1.013. Thus DNA weighted irradiance can be overestimated by up to 4%, if the bandwidth of the spectroradiometer is 2 nm FWHM and no corrections are applied.

The factors $R_{R,\mathrm{Bio}}(B)$ were found to depend almost quadratically on bandwidth B and thus can be approximated by $R^{\star}_{R,\mathrm{Bio}}(B)$:

$$R^{\star}_{R,\mathrm{Bio}}(B) = 1 + [R_{R,\mathrm{Bio}}(1\,\mathrm{nm}) - 1]\,B^2, \qquad (20)$$

where B is in nanometers. For bandwidths between 0.5 and 2.0 nm, $[R_{R,\mathrm{DNA}}(B) - 1]$ and $[R^{\star}_{R,\mathrm{DNA}}(B) - 1]$ agree to within ±5%. To illustrate the good agreement, $R^{\star}_{R,\mathrm{DNA}}(2\,\mathrm{nm})$ is drawn in Figure 3 as well.

In Table 2, $R_{R,\mathrm{DNA}}(1\,\mathrm{nm})$ and the analogous quantity for erythemal weighting, $R_{R,\mathrm{Ery}}(1\,\mathrm{nm})$, are given for several solar elevations and ozone values. With (20) these values can be estimated for triangular slit functions with bandwidths in between 0.5 and 2.0 nm with an accuracy of better than ±5%.

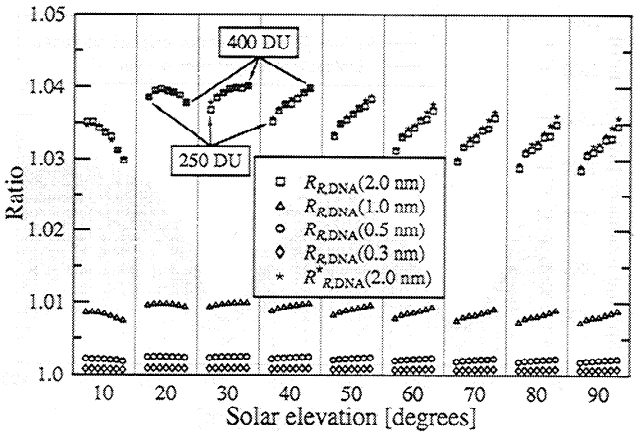

Figure 3. Effect of resolution on DNA weighted irradiance. Shown are ratios $R_{R,\mathrm{DNA}}(B)$ of measured and "true" DNA weighted irradiance as a function of solar elevation and total ozone for four different bandwidths between 0.3 and 2.0 nm. For each solar elevation a subset of seven data points is drawn, referring to the ozone values of (left to right) 250, 280, 300, 320, 340, 370, and 400 DU. The ratios $R^{\star}_{R,\mathrm{DNA}}(2\,\mathrm{nm})$ approximate $R_{R,\mathrm{DNA}}(2\,\mathrm{nm})$ according to equation (20).

3.3.2. Spectral irradiance errors caused by the resolution of the spectroradiometer. The ratio of spectral irradiance measured with a spectroradiometer with slit function $f(\lambda)$ and the "true" spectral irradiance is $R_R(\lambda, B) = E_R(\lambda, f)/E(\lambda)$, where, again, B is the bandwidth of the slit function $f(\lambda)$. Owing to the Fraunhofer fine structure, these ratios vary on a 0.001 nm scale. Because of this spectral structure,

Table 2. Parameters to Calculate Errors Caused by Finite Resolution of a Spectroradiometer[a] and Wavelength Shifts[b] on Dependence of Solar Elevation (Sh) and Total Ozone (Oz)

Sh	Oz, DU	$R_{R,\mathrm{DNA}}$(1nm)	$R_{R,\mathrm{Ery}}$(1nm)	$c_{R,1}$	$c_{R,2}$	$R_{W,\mathrm{DNA}}$(0.1nm)	$R_{W,\mathrm{Ery}}$(0.1nm)	$c_{W,1}$	$c_{W,2}$
10	250	1.00866	1.00252	265.26	9.16	1.0319	1.0148	255.43	15.42
10	320	1.00846	1.00225	274.00	7.88	1.0300	1.0133	263.71	13.83
10	400	1.00751	1.00196	281.70	6.53	1.0271	1.0119	269.48	12.76
30	250	1.00943	1.00325	282.77	4.86	1.0345	1.0186	274.61	9.21
30	320	1.00992	1.00313	287.39	4.22	1.0349	1.0177	278.91	8.51
30	400	1.01004	1.00294	290.99	3.69	1.0344	1.0167	281.63	8.18
50	250	1.00835	1.00320	283.25	3.94	1.0331	1.0195	274.03	8.51
50	320	1.00912	1.00331	285.46	3.91	1.0343	1.0192	276.69	8.28
50	400	1.00969	1.00327	287.36	3.88	1.0349	1.0186	279.01	8.08
70	250	1.00753	1.00299	281.09	4.06	1.0319	1.0194	271.31	8.86
70	320	1.00835	1.00322	283.52	3.98	1.0333	1.0195	274.56	8.46
70	400	1.00915	1.00332	285.01	4.08	1.0343	1.0192	276.62	8.36
90	250	1.00725	1.00290	280.84	3.98	1.0314	1.0193	271.07	8.77
90	320	1.00806	1.00317	283.23	3.91	1.0330	1.0195	273.96	8.50
90	400	1.00893	1.00331	284.52	4.06	1.0341	1.0193	276.46	8.24
Mean[c]		1.00888	1.00305	...	...	1.0333	1.0180	...	...
Standard deviation[c]		0.00077	0.00034	...	...	0.0016	0.0020	...	...

[a]See section 3.3.
[b]See section 3.4.
[c]Means and standard deviations of the parameters are given over the whole ranges of solar elevations (10° - 90°) and ozone columns (250 - 400 DU).

Webb et al. [1998] conclude that uncertainties caused by the slit function cannot easily be defined. In order to parameterize the systematic overestimate of the true solar spectrum at short wavelengths caused by the slit function, we have fitted exponential functions $R_R^*(\lambda, B)$ to the ratios $R_R(\lambda, B)$. With these fits the general slope of $R_R(\lambda, B)$ at the ozone cutoff and the dependence of this ratio on solar elevation and total ozone are illustrated:

$$R_R^*(\lambda, B) = 1 + \{\exp[(c_{R,1} - \lambda)/c_{R,2}]\}\, B^2, \quad (21)$$

where $c_{R,1}$ and $c_{R,2}$ are coefficients depending on solar elevation and ozone, respectively, and λ and B have to be set in nanometers; $c_{R,1}$ and $c_{R,2}$ are given in Table 2.

The definition of smooth fit functions is reasonable because systematic errors in biologically weighted irradiance calculated with these functions agree well with the correct calculation using (18): for a bandwidth of 1 nm the avarage value of $R_{R,\mathrm{DNA}}(1\,\mathrm{nm})$ calculated with (18) is 1.00888 ± 0.00077 (see Table 2). If $E_R(\lambda, f)$ in (18) is substituted by the approximation $E(\lambda)\, R_R^*(\lambda, 1\mathrm{nm})$ and $R_{R,\mathrm{DNA}}(1\,\mathrm{nm})$ is calculated again, the result is 1.00991 ± 0.00137.

In Figure 4, $R_R^*(\lambda, 1\,\mathrm{nm})$ is shown for three different solar elevations and ozone columns between 250 and 400 DU. Generally, the ratios increase strongly when λ decreases: at 300 nm, 30° solar elevation, and 400 DU, $R_R^*(\lambda, 1\,\mathrm{nm})$ is 1.087, whereas at 315 nm the ratio is almost 1. With increasing solar elevation or decreasing ozone the curves are shifted toward shorter wavelengths.

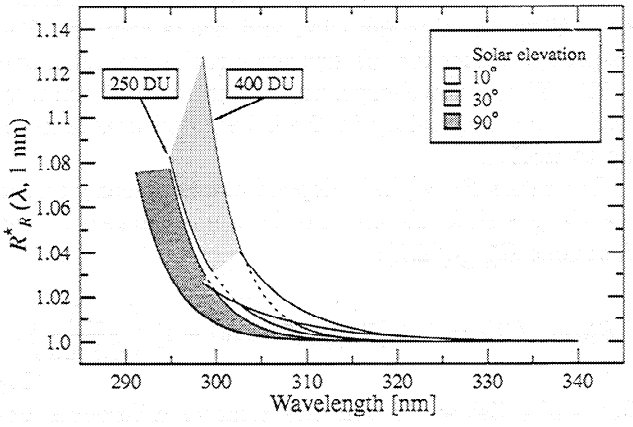

Figure 4. Effect of bandwidth on spectral irradiance. Shown are ratios of measured and true spectral irradiance approximated by the exponential fit functions $R_R^*(\lambda, B)$, which are given in equation (21). The ratios were calculated with a triangular slit function of 1 nm FWHM and are shown for three different solar elevations and ozone columns. The shaded areas refer to solar elevations of 10°, 30°, and 90°. The left boundary of each area refers to 250 DU; the right boundary refers to 400 DU. For 10° and 30° the shortwave ends of the shaded areas refer to a spectral irradiance $E(\lambda)$ of 0.01 mW/(m^2 nm); for 90° solar elevation the boundary spectral irradiance is 0.1 mW/(m^2 nm).

3.3.3. Effect of nontriangular slit functions. Up until now, only symmetrical slit functions of triangular shape were considered. Slit functions of actual spectroradiometers usually deviate from this ideal shape and are a mixture of triangular and Gaussian functions. Sensitivity studies have shown that the conclusions drawn above remain valid when the slit function is of Gaussian shape [*Bernhard*, 1997]. For example, at 70° solar elevation and 320 DU, $R_{R,\mathrm{DNA}}(1\,\mathrm{nm})$ is 1.00835 for a triangular slit function of 1 nm FWHM and 1.00801 for a slit function of the same bandwidth, but of Gaussian shape. However, if the slit function of an instrument appears to deviate significantly from either shapes, the measurement errors have to be calculated explicitly with (17) and (18). In particular, instruments with an asymmerical slit function have to be treated with special care. Here the influence of slit function is mixed with the wavelength misalignment.

3.4. Wavelength Misalignment

Because of the strong decline of the solar spectrum in the UVB, small errors in the wavelength alignment of a spectroradiometer lead to significant errors in measured spectral irradiance. If a wavelength shift at a specific wavelength is well defined, the resulting systematic errors can be corrected. However, in practice, the shift is only known within certain limits (e.g., ±0.05 nm), leading to uncertainties in irradiance readings.

Usually, the wavelength setting of a spectroradiometer is calibrated by measuring the spectrum of a line source, e.g., a low-pressure mercury lamp, the line position of which is known to within ±0.001 nm [*Lide et al.*, 1990]. Comparing measured and actual line positions, a wavelength scale is assigned to the monochromator. For several reasons, there still remain uncertainties in the wavelength calibration after this procedure: (1) Since the wavelength calibration is based only on several lines, the calibration for wavelengths in between may be in error if, e.g., the wavelength drive of the monochromator exhibits nonlinearities. (2) Owing to mechanical or temperature dependent instabilities, the wavelength setting of the monochromator may change with time. (3) If the slit function is asymmetrical, the center of the line is ambiguous.

As an alternative to the use of spectral lamps, the wavelength calibration can be carried out by correlating the Fraunhofer structure in segments of the measured spectra with the respective structure in reference solar spectra, e.g., an extraterrestrial spectrum derived from satellite data or high-resolution ground-based data. Possible implementations are described by *Huber et al.* [1993], *Slaper et al.* [1995], and *Mayer* [1997]. Note that these methods require the knowledge of the slit function of the instrument and may not be suitable for instruments with array detectors, where a measurement of the slit function is not always possible [*Seckmeyer et al.*, 1998]. The accuracy of such methods

is limited by the wavelength accuracy of the reference spectrum. However, if an appropriate spectrum is used, wavelength uncertainties can be reduced to ±0.02 nm for wavelengths above 310 nm [*Webb*, 1997]. Below 310 nm the accuracy may be limited because the structures in the ozone cross section interfere with the Fraunhofer structure. Appropriate reference spectra are the Kitt Peak spectrum [*Kurucz et al.*, 1984], introduced in section 3.3, or the extraterrestrial spectrum measured by the Solar Ultraviolet Spectral Irradiance Monitor (SUSIM) on board the Atmospheric Laboratory for Applications and Science (ATLAS 3) platform [*Kaye and Miller*, 1996]. The spectrum is available from the ftp server susim.nrl.navy.mil (personal communication, M. VanHoosier, 1996).

Although wavelength errors can be reduced by appropriate methods, intercomparison campaigns of UV spectroradiometers carried out in the past have revealed wavelength shifts of up to ±0.5 nm [*Bais*, 1998; *Seckmeyer et al.*, 1998]. The consequences of such shifts are quantified in the following. For this purpose, $E_{W,R}(\lambda, \Delta\lambda)$ is defined as the measured irradiance of a spectroradiometer, which has an error in the wavelength setting of $\Delta\lambda$. $E_R(\lambda)$ is the respective irradiance reading of an identical instrument with no wavelength shifts. The error ratio $R_{W,R}(\lambda, \Delta\lambda)$ of both measurements is then

$$R_{W,R}(\lambda, \Delta\lambda) = \frac{E_{W,R}(\lambda, \Delta\lambda)}{E_R(\lambda)} = \frac{E_R(\lambda + \Delta\lambda)}{E_R(\lambda)} \quad (22)$$

Note that $E_R(\lambda)$ is the irradiance convolved with the instrument's slit function. Thus (22) describes the influence of wavelength misalignment on a practical instrument with finite resolution. Since $E_R(\lambda)$ depends on bandwidth so does $R_{W,R}(\lambda, \Delta\lambda)$: for an instrument with small bandwidth, the ratios contain more noise than those for an instrument that has a broad slit function. Owing to this noise, procedures similar to those in section 3.3 are necessary to quantify the effects of wavelength shifts on spectral irradiance in the ozone cutoff and to quantify errors in measured biologically weighted irradiances.

3.4.1. Errors in measurements of biologically weighted irradiance caused by wavelength shifts. In analogy to section 3.3.1, the quantity $R_{W,\mathrm{Bio}}(\Delta\lambda)$ is defined to study the effect of wavelength shifts on biologically weighted irradiance. $R_{W,\mathrm{Bio}}(\Delta\lambda)$ is the ratio of biologically weighted irradiance measured with an instrument with wavelength shift $\Delta\lambda$ to measurements of an identical instrument with no shifts:

$$R_{W,\mathrm{Bio}}(\Delta\lambda) = \frac{\int_0^\infty E_{W,R}(\lambda, \Delta\lambda)\, A_{\mathrm{Bio}}(\lambda)\, d\lambda}{\int_0^\infty E_R(\lambda)\, A_{\mathrm{Bio}}(\lambda)\, d\lambda} \quad (23)$$

The error ratios for DNA and erythemal weighting are denoted $R_{W,\mathrm{DNA}}(\Delta\lambda)$ and $R_{W,\mathrm{Ery}}(\Delta\lambda)$, respectively. Apart from the dependence on $\Delta\lambda$, $R_{W,\mathrm{Bio}}(\Delta\lambda)$ depends mainly on solar elevation and total ozone.

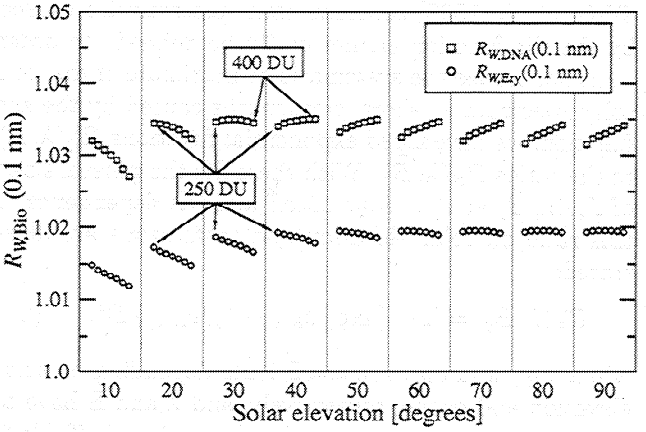

Figure 5. Effect of wavelength misalignment on measurements of biologically weighted irradiance. The top curve shows the error ratio $R_{W,\mathrm{DNA}}(0.1\,\mathrm{nm})$ of measured and true DNA weighted irradiance as a function of solar elevation and total ozone for 0.1 nm wavelength shift. The bottom curve is the ratio for erythemal irradiance. For each solar elevation a subset of seven data points is drawn, referring to the ozone values of (left to right) 250, 280, 300, 320, 340, 370, and 400 DU.

For $\Delta\lambda < 0$, $R_{W,\mathrm{Bio}}$ is usually smaller than 1; for $\Delta\lambda > 0$ the ratio is larger than 1. This is in contrast to $R_{R,\mathrm{Bio}}(B)$, since the influence of the slit function always leads to an overestimate of weighted irradiances near the ozone cutoff.

In Figure 5, the error ratios for DNA and erythemally weighted irradiance are shown. For a shift of 0.1 nm the DNA weighted ratios vary between 1.027 and 1.035, depending on solar elevation and ozone column. The respective values for the erythema ratios are 1.012 and 1.020. Thus a wavelength uncertainty of ±0.1 nm may lead to an uncertainty in DNA weighted irradiance of up to ±3.5%.

The ratios $R_{W,\mathrm{Bio}}(\Delta\lambda)$ depend almost linearly on the wavelength shift $\Delta\lambda$ and can be approximated by the functions $R^*_{W,\mathrm{Bio}}(\Delta\lambda)$:

$$R^*_{W,\mathrm{Bio}}(\Delta\lambda) = 1 + [R_{R,\mathrm{Bio}}(0.1\,\mathrm{nm}) - 1]\left(\frac{\Delta\lambda}{0.1\,\mathrm{nm}}\right). \quad (24)$$

For shifts below 0.3 nm the relative differences between $[R_{W,\mathrm{Bio}}(\Delta\lambda) - 1]$ and $[R^*_{W,\mathrm{Bio}}(\Delta\lambda) - 1]$ are smaller than ±4% for DNA weighting and ±2% for erythemal weighting, respectively. For shifts as large as 0.5 nm the approximation may be wrong by about 7% (DNA weighting) and 4% (erythema weighting). In Table 2, $R_{W,\mathrm{DNA}}(0.1\,\mathrm{nm})$ and $R_{W,\mathrm{Ery}}(0.1\,\mathrm{nm})$ are given for several solar elevations and ozone values. With (24) these values can be calculated reasonably well for shifts of up to 0.3 nm.

The dependence of $E_R(\lambda)$ on bandwidth leads also to small variations in $R_{W,\mathrm{Bio}}(\Delta\lambda)$. However, in practice, these changes are negligible: the maximum difference

in $R_{W,\mathrm{DNA}}(0.1\,\mathrm{nm})$ calculated separately for 0.3 and 2.0 nm bandwidth is smaller than 0.0003 for all solar elevations and ozone columns considered.

3.4.2. Spectral irradiance errors caused by wavelength shifts and the Fraunhofer structure. The ratio $R_{W,R}(\lambda, \Delta\lambda)$ shows a large wavelength dependence because of the Fraunhofer structure. The average variability in a given wavelength interval $[\lambda_0 - \delta\lambda, \lambda_0 + \delta\lambda]$ is quantified by the standard deviation $\sigma_F(\lambda_0, \delta\lambda)$:

$$\sigma_F(\lambda_0, \delta\lambda) = \sqrt{\frac{1}{n-1} \sum_{\lambda_i \in [\lambda_0 \pm \delta\lambda]} [R_{W,R}(\lambda_i, \Delta\lambda) - 1]^2}, \quad (25)$$

where the ratios $R_{W,R}(\lambda_i, \Delta\lambda)$ are calculated at discrete wavelengths λ_i. Since the Fraunhofer lines are not uniformly distributed, $\sigma_F(\lambda_0, \delta\lambda)$ depends on the center wavelength λ_0 and the width of the interval. For example, σ_F is larger in the vicinity of the calcium doublet at 395 nm than in the region of 382 nm [*Bernhard et al.*, 1998].

The standard uncertainty of $E(\lambda)$ caused by wavelength shifts and the Fraunhofer structure is described here by $u_F(\lambda) = \sigma_F(\lambda, \delta\lambda)\, E(\lambda)$, where $\sigma_F(\lambda, \delta\lambda)$ is calculated over a 10 nm interval; that is, $\delta\lambda = 5$ nm. Thus the standard uncertainty $u_F(\lambda)$ is a smooth function of wavelength and is therefore comparable to other uncertainties in solar measurements. An example of the magnitude and wavelength variability of u_F is given in section 4.4 and Figure 8.

3.4.3. Spectral irradiance errors caused by wavelength shifts in the ozone cutoff. In order to quantify the influence of wavelength shifts on UV measurements in the ozone cutoff, we use similar fit functions as proposed in the last section. These fit functions are denoted $R^*_{W,R}(\lambda, \Delta\lambda)$ and are defined by

$$R^*_{W,R}(\lambda, \Delta\lambda) = 1 + \{\exp[(c_{W,1} - \lambda)/c_{W,2}]\} \frac{\Delta\lambda}{0.1\mathrm{nm}}, \quad (26)$$

where $c_{W,1}$ and $c_{W,2}$ are coefficients depending on solar elevation and ozone, respectively. $c_{W,1}$ and $c_{W,2}$ are given in Table 2. The approximation is applicable for wavelength shifts smaller than ± 0.3 nm and bandwidths below 2.0 nm. For larger bandwidths the effects of wavelength shifts and the slit function can no longer be treated independently.

In Figure 6, $R^*_{W,R}(\lambda, 0.1\,\mathrm{nm})$ is shown for three different solar elevations and ozone columns between 250 and 400 DU. In all cases the error ratios increase strongly when λ decreases. With increasing solar elevation or decreasing ozone column, the ratios are shifted to shorter wavelengths.

Errors in DNA weighted irradiances estimated with the proposed fit functions $R^*_{W,R}(\lambda, \Delta\lambda)$ agree well with the correct error ratios $R_{W,\mathrm{DNA}}(\Delta\lambda)$: for a wavelength shift of 0.1 nm the average value of $R_{W,\mathrm{DNA}}(0.1\,\mathrm{nm})$ calculated with (23) is 1.0333 ± 0.0016 (see Table 2). If $E_{W,R}(\lambda, \Delta\lambda)$ is substituted in (23) by the approximation $E_R(\lambda)\, R^*_{W,R}(\lambda, \Delta\lambda)$, and $R_{W,\mathrm{DNA}}(0.1\,\mathrm{nm})$ is recalculated, the result is 1.0334 ± 0.0022. The deviation of both calculations is less than 1%. This demonstrates that the definition of a smooth fit function is meaningful, although this approach neglects the influence of the Fraunhofer structure.

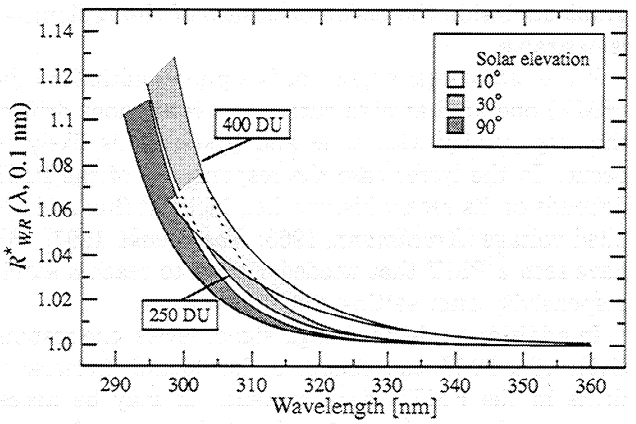

Figure 6. Ratio of wavelength-shifted and -unshifted spectral irradiance approximated by the exponential fit functions $R^*_{W,R}(\lambda, \Delta\lambda)$ given in (26). The ratios were calculated for a wavelength shift of 0.1 nm and a bandwidth of 1.0 nm FWHM and are shown for three different solar elevations and different ozone columns. The shaded areas refer to solar elevations of 10°, 30°, and 90°. The left boundary of each area refers to 250 DU; the right boundary refer to 400 DU. For 10° and 30° the shortwave ends of the shaded areas refer to a spectral irradiance $E(\lambda)$ of 0.01 mW/(m^2 nm); for 90° solar elevation the boundary spectral irradiance is 0.1 mW/(m^2 nm).

3.5. Radiometric Stability

Possible reasons for instabilities of the radiometer's spectral responsivity include contamination of the entrance optics, change of the detector's responsivity, and change of the monochromator throughput. Instabilities in the monochromator/detector part are often caused by changes in the environment, namely temperature, humidity, magnetic and electrostatic fields, power cuts, or ground loops. Changes in temperature can also alter the monochromator's wavelength alignment. A thorough laboratory characterization of a spectroradiometer's temperature dependence with respect to both radiometric and wavelength stability has been compiled by T. M. Thorseth (Proceedings of the first internet conference on Photochemistry and Photobiology, Nov 17 - Dec 19, 1997, http://www.photobiology.com/v1/thorseth/index.htm, 1997). However, temperature coefficients derived in the laboratory can change with time, e.g., due to mechanical wear and tear, and therefore a good temperature stabilization with low temperature

gradients inside the entire enclosure of the radiometer is desirable.

If the radiometer's detector is a photomultiplier tube (PMT) operated at high currents, a continuous drift of the responsivity with time and hysteresis is likely to occur. In the latter case the responsivity of the PMT depends on its recent history, i.e., incident flux and applied voltage [*Krochmann*, 1963; *Kostkowski*, 1997]. We have seen a PMT that needed 1 week to reach a stable responsivity after setting the high voltage.

In addition to drifts at high signal levels, the responsivity of a PMT can change at low signals because of drifts in the PMT's dark current. It may be necessary therefore to determine the dark current for each measurement and subtract it from the signal. By chopping the radiation falling on the PMT and using a lock-in amplifier or by operating a PMT in photocounting mode, such offset drifts can be effectively suppressed [*Kostkowski*, 1997].

An internal lamp to regularly monitor the responsivity of a radiometer is helpful to track instrument drifts caused by monochromator or detector [*Booth et al.*, 1994]. However, in our experience, the main contribution to instabilities in a high-quality spectroradiometer originates from contamination of the entrance optics. Only by regular calibration of the whole system (e.g., on a weekly basis) can these drifts be quantified.

The standard deviation of the calibration records allows an assessment of the stability of the instrument over a specific time period (e.g., a year). However, since only drifts between two calibrations contribute to the uncertainty at a particular time, the standard uncertainty arising from radiometric instabilities is the standard deviation of the difference of consecutive calibrations; see section 4.5.

3.6. Nonlinearity

The signal of a radiometer should be proportional to the incident flux. The ratio $R_N(\lambda)$ of spectral irradiance measured with a radiometer, which exhibits nonlinearities, to the true irradiance can be determined with two light sources, L_1 and L_2, of different but known radiative power. The irradiances E_1 and E_2 of these sources produce instrument signals S_1 and S_2. If E_1 is the irradiance at the calibration level of the instrument, $R_N(\lambda)$ is then calculated according to

$$R_N(\lambda, S_2) = \frac{E_1(\lambda)}{S_1(\lambda)} \frac{S_2(\lambda)}{E_2(\lambda)}. \tag{27}$$

To minimize errors in the determination of $R_N(\lambda, S_2)$, L_1 and L_2 should differ only in their radiative power; their spectral distribution and the geometries of their radiation fields must resemble each other. A point source set at two different distances fulfills this requirement. The inverse square law can then be used to determine $R_N(\lambda)$ by varying the distance between the point source and the radiometer and measuring simultaneously $S_2(\lambda)$ [*Kostkowski*, 1997]. A comprehensive overview of other methods to determine and to correct nonlinearities has been complied by *Sanders* [1972]. An automatic linearity tester was introduced by *Saunders and Shumaker* [1984].

Nonlinearity is of special concern in solar UV radiometry because the level of solar radiation deviates much from the level of calibration sources: for wavelengths above 330 nm the solar spectrum irradiance is typically 2 to 3 orders of magnitude higher than the irradiance of an FEL lamp. In contrast, for wavelengths below 300 nm the solar spectrum can be lower than the lamp by more than 3 orders of magnitude.

The main cause of nonlinearity is saturation of the detector. For PMTs, significant nonlinearity usually occurs if the anode current is higher than 1 μA.

Nonlinearities may also appear if a PMT is operated at different high voltage within a spectrum or if the gain of the detector electronics is switched during a scan. In these cases, sudden changes in linearity may occur, see section 4.6. Polynomial fit functions, which are usually applied to correct nonlinearities [*Kostkowski*, 1997], are not applicable in these cases. A method to detect such nonlinearities in data of solar irradiance was described by *Bernhard et al.* [1998].

3.7. Noise

Owing to noise in the radiometer signal, several measurements of the same irradiance will lead to different results. Usually, the signal-to-noise ratio S/N, which is the ratio of the radiometer's average signal divided by the standard deviation of this signal, is used to quantify the influence of noise. For a spectroradiometer with a PMT detector, the noise is mainly caused by "shot noise," which results from the discrete nature of the electrons leaving the PMT's cathode. For signal levels, where the dark current of the PMT is negligible, S/N is determined by Poisson statistics resulting in

$$\mathrm{S/N} \approx \sqrt{\Phi_p Q t_s}, \tag{28}$$

where Φ_p is the incident photon flux, Q is the quantum efficiency of the PMT's photo cathode, and t_s is the sampling time. In this case, S/N is proportional to the square root of the radiometer's signal. Other sources of noise, such as noise from the dynodes of the PMT, noise introduced by the amplifier, or digitization noise, can slightly increase the S/N ratio given in (28). For more information, see *Kostkowski* [1997], where the noise for photodiode and multichannel detectors is also estimated.

The S/N ratio can be derived from consecutive measurements of a stable light source. By varying the distance to the source, S/N can be measured at different signal levels.

The standard uncertainty $u_N(\lambda)$ in a measurement of spectral irradiance that is due to noise depends on the noise during calibration and during the measurement of

the unknown source. Using (2), (9), and the definition of the signal-to-noise ratio, $u_N(\lambda)$ is given by

$$u_N(\lambda) = \left(\left[\frac{E_L(\lambda)}{S_L(\lambda)} \right]^2 \left\{ \frac{S_M(\lambda)}{\mathrm{S/N}[S_M(\lambda)]} \right\}^2 + \left[\frac{S_M(\lambda) E_L(\lambda)}{S_L^2(\lambda)} \right]^2 \left\{ \frac{S_L(\lambda)}{\mathrm{S/N}[S_L(\lambda)]} \right\}^2 \right)^{1/2}, \quad (29)$$

where $E_L(\lambda)$ and $E_M(\lambda)$ are the irradiances produced by calibration lamp and unknown source, respectively; $S_L(\lambda)$ and $S_M(\lambda)$ are the corresponding signals; and $\mathrm{S/N}[S_L(\lambda)]$ and $\mathrm{S/N}[S_M(\lambda)]$ are the signal-to-noise ratios at both signals.

If biologically weighted irradiances E_{Bio} are calculated from spectral measurements, the uncertainty due to noise is significantly reduced. E_{Bio} can be approximated by the sum

$$E_{\mathrm{Bio}} = \sum_i E(\lambda_i)\, A(\lambda_i)\, (\lambda_{i+1} - \lambda_i), \quad (30)$$

where $A_{\mathrm{Bio}}(\lambda)$ is the relevant action spectrum and the sum is over all discrete wavelengths λ_i measured by the spectroradiometer. The standard uncertainty $u_{N_{\mathrm{Bio}}}$ of E_{Bio} is then

$$u_{N_{\mathrm{Bio}}} = \sqrt{\sum_i \{u_N(\lambda_i)\, A(\lambda_i)\, (\lambda_{i+1} - \lambda_i)\}^2}, \quad (31)$$

where $u_N(\lambda_i)$ is the standard uncertainty at wavelength λ_i, calculated with (29). By summing over the wavelengths, $u_{N_{\mathrm{Bio}}}/E_{\mathrm{Bio}}$ is significantly reduced compared to $u_N/E(\lambda)$.

The detection limit of a spectroradiometer is limited either by stray light (see next section) or by noise, if the integration time is fixed. In the latter case the detection limit is reached if $\mathrm{S/N}(\lambda) = 1$. The minimal irradiance that can be measured at a wavelength λ is the "noise equivalent irradiance" (NEI) that is defined by the ratio of the standard deviation σ_{Dark} of the radiometer's dark signal to the responsivity $r(\lambda)$ at wavelength λ

$$\mathrm{NEI}(\lambda) = \sigma_{\mathrm{Dark}}/r(\lambda) \quad (32)$$

3.8. Stray Light

Stray light is radiation at wavelengths outside the wavelength range of the slit function that is detected together with radiation inside this range. Since the wavelength limits of a slit function cannot be unambigously defined, some authors introduced the term "slit-scattering function," which comprises both the slit function (in the meaning of the previous sections) and its long-wavelength wings (or background), which contribute to stray light [*Kostkowski*, 1997]. For good double monochromators this background level is more than 9 orders of magnitude below the peak of the slit-scattering function. The measurement of stray light 9 orders of magnitude below the maximum is a demanding task: it requires a sufficiently powerful line source (e.g., a HeCd laser operating at 325 nm) and additional facilities to suppress the radiation continuum of the source.

According to the *Commission Internationale de l'Éclairage* [1984], the amount of stray light in a spectroradiometer depends, among other factors, on the quality and cleanness of all optical surfaces (mirrors and gratings), bandwidth, wavelength, the spectral response of the detector, the spectral transmittance of the monochromator and all auxiliary optics, and the spectral distribution of the source. In the presence of stray light the measured solar spectrum does not follow the steep decrease in the ozone cutoff down to the radiometer's noise level but turns into approximately constant values at short wavelengths. Although such behavior can also be caused by an electronic offset, the effects can be distinguished by covering the entrance optics: if the signal in the shortwave end of the spectrum remains constant, the offset is caused by the electronics.

In the case of stray light the ratio $R_{\mathrm{Str}}(\lambda)$ of measured to true irradiance $E(\lambda)$ is

$$R_{\mathrm{Str}}(\lambda) = \frac{E_{\mathrm{Str}}(\lambda) + E(\lambda)}{E(\lambda)} = 1 + \frac{E_{\mathrm{Str}}(\lambda)}{E(\lambda)}, \quad (33)$$

where $E_{\mathrm{Str}}(\lambda)$ is the contribution to the measured irradiance at wavelength λ that originates from radiation at wavelengths outside the range of the slit function.

Below 285 nm, virtually no radiation reaches the Earth's surface owing to ozone absorption. Consequently, if measurements of solar spectral irradiance below 285 nm are above the noise level of the instrument, they originate from stray light. Thus measurements at wavelengths below 285 nm can be used to estimate $E_{\mathrm{Str}}(\lambda)$. The extrapolation of $E_{\mathrm{Str}}(\lambda)$ to wavelengths above 285 nm allows a correction to the measurement result to be made. This method has been applied to single Brewer spectrophotometers [*Köhler et al.*, 1995; *Bais et al.*, 1996]. Since stray light is usually wavelength dependent, the accuracy of corrections based on extrapolation procedures is limited.

Instead of using the solar spectrum, stray light can also be determined with an artificial light source and cutoff filters. With several filters of different cutoff wavelengths the spectral distribution of stray light can be roughly determined [*Commission Internationale de l'Éclairage*, 1984]. Results from those characterizations can only be transferred to solar measurements if the filtered artificial spectrum is similar in shape to the solar spectrum.

3.9. Timing Errors

Since computer clocks are often inaccurate, the time that is assigned to each wavelength of a solar spectrum may be in error. This problem can be solved by installing radio clocks or using the time signal from a

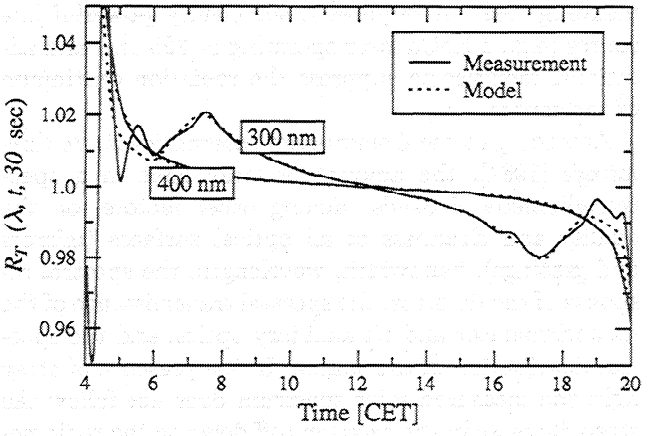

Figure 7. Effect of time shifts on spectral measurements. Shown are ratios $R_T(\lambda, t, 30\text{ s})$ of shifted/unshifted spectral irradiance at 300 and 400 nm. The shift applied was 30 s. The solid lines are based on measurements conducted on July 22, 1996, in Garmisch-Partenkirchen. The dotted lines represent the corresponding modeled ratio.

Global Positioning System (GPS), but time shifts exist in many measurements. They can be quantified only if the magnitude of the shift Δt is known. The ratio of measurements that suffer from an incorrect clock and the true irradiance is

$$R_T(\lambda, t, \Delta t) = \frac{E(\lambda, t + \Delta t)}{E(\lambda, t)}. \quad (34)$$

Figure 7 shows ratios $R_T(\lambda, t, 30\text{ s})$ for a time shift of $\Delta t = 30$ s applied deliberately to spectral measurements of the mobile IFU spectroradiometer conducted on the clear-sky day, July 22, 1996, at 300 and 400 nm. Figure 7 also shows the ratios obtained with the model. It is clear from the plot that measurements at 300 nm are affected more by time shifts than measurements at 400 nm. This is because shorter wavelengths show a stronger variation with solar zenith angle, owing to the wavelength dependence of ozone absorption and Rayleigh scattering. For 300 nm the time shift of 30 s results in systematic errors of ±2% at 0700 and 1700 CET for the given day.

3.10. Other Sources of Uncertainty

If an array detector is used instead of a PMT, cross talk between array cells must be considered. A good summary of the characteristics of array detectors is given by *Kostkowski* [1997].

Ideally, the signal $S_M(\lambda)$ of a radiometer should follow instantaneously the change of the incident radiation. Practical detectors and amplifiers have a time constant τ_0. A sufficiently long waiting time is therefore required before the measurement at a new wavelength starts.

In order to correct for a potential electronic offset (that is, the signal deviates from zero if no radiation is falling on the instrument), the offset must be determined before a spectral scan and then substracted from the signal. If the offset changes with time, the measurement is associated with an uncertainty. Offset drifts caused by a PMT mainly influence measurements at low signals, namely, measurements of solar spectra at short wavelengths or near the detection limit. Drifts are therefore less critical during calibration. By measuring the offset before and after the scan of a solar spectrum, the standard uncertainty in the measured irradiance can be estimated with (7).

For several reasons, e.g., interference between different parts of the electronics, randomly scattered spikes can appear in a radiometer's signal. A method to detect such features has been proposed by *Bernhard et al.* [1998].

A further source of error, which has consequences similar to the cosine error, is incorrect leveling of the entrance optics at the measurement site. This error arises mostly from the wrong weighting of direct irradiance rather than sky irradiance. With a good spirit level the optics can be adjusted to within a standard uncertainty of ±0.1°. For 60° SZA, 400 nm, and no aerosols, this leads to a standard uncertainty of 0.2% in the irradiance. For shorter wavelengths the uncertainty decreases owing to a smaller contribution from direct irradiance.

3.11. Combined uncertainty

On the basis of a thorough instrument characterization, the different uncertainties of solar UV radiometry described in the last sections can be determined and, finally, the combined uncertainty u_{comb} can be calculated with (8). By multiplying the result with the coverage factor $k = 2$, the expanded uncertainty U is obtained.

4. Uncertainty of Mobile IFU Spectroradiometer

The methodologies to derive the overall uncertainty of UV spectroradiometers introduced in the last sections are now applied to the mobile IFU spectroradiometer, referred to hereafter as "IFU radiometer." This instrument uses newly developed entrance optics, described by *Bernhard and Seckmeyer* [1997], which are coupled by a quartz fiber to a Bentham DTM300 double monochromator. The (measured) bandwidth of the instrument is 0.574 nm FWHM. Radiation leaving the monochromator is chopped, detected with a PMT, and amplified using the lock-in technique. The system is temperature stabilized and under full PC control. The data are routinely corrected for the cosine error. The IFU radiometer has successfully participated in several international intercomparisons of UV spectroradiometers [*Webb*, 1997; *Bais*, 1998; *Seckmeyer et al.*, 1998]. More details on the instrument were compiled by *Seckmeyer et al.* [1996], *Bernhard et al.* [1997], and *Bernhard et al.* [1998].

4.1. Radiometric Calibration

Field calibrations of the IFU radiometer are made with 100 W M28 working standards. These lamps are calibrated before use with a collection of four FEL 1000 W reference standard lamps of type T6 that have certificates issued by PTB. The IFU radiometer is used in the laboratory of IFU to transfer the calibration from the collective standard to the 100 W lamps. Consequently, uncertainties in the field calibration of the instrument comprise uncertainties arising from the transfer and from the use of the working standards. In Table 3, all contributions to the calibration uncertainty are compiled and are further explained in the following references:

1. Reference 1 is the uncertainty caused by the spline interpolation of the calibration points of reference standards to wavelengths in between these points (see section 3.1.5).

2. The 100 W working standards are calibrated at a distance of 50 cm but used at a distance of 37 cm in a specially designed lamp housing. The irradiance values referring to 50 cm are scaled with the inverse square law. Separate measurements of the lamp at both distances have confirmed that the scaling factor is accurate to within ±0.3%.

3. The entrance optics of the instrument are based on a non planar diffuser. The location of the reference plane of this diffuser, which is relevant for the measurement of the correct distance between diffuser and calibration lamp, is uncertain by ±0.4 mm. This leads to a standard uncertainty of 0.2% in the irradiance (section 3.1.4).

4. The instrument's entrance optics are protected by a quartz dome. The refraction of incident radiation at the dome was calculated and causes an uncertainty of 0.2% (section 3.1.4).

5. PTB's calibration certificates refer to a receiver area of 20 mm × 10 mm. The area of the diffuser used in the laboratory to transfer the calibration of the PTB reference standards to the working standards has a diameter of only 5 mm, causing an uncertainty of 0.1%.

6. References 6 and 7 concern the distance between lamp and reference plane of the entrance optics, which can be measured only to within ±0.3 mm, causing a standard uncertainty of 0.1% for both the FEL reference standard and 100 W working standard.

7. References 8-10 give the uncertainty caused by further alignment errors of the lamps or the entrance optics. The uncertainties are similar to the values described by *Sperling et al.* [1996]; see section 3.1.3.

8. In references 11 and 12, although a high-quality current source is used, the lamp current of both FEL reference lamps and 100 W working standards can only be set to within ±0.01%, resulting in a standard uncertainty in the irradiance of 0.1% (section 3.1.3).

9. In reference 13, each lamp of the IFU collective standard is in use for about 2 hours per year. Since the lamp drift is estimated to be less than 0.01%/hour (section 3.1.2), the irradiance scale at IFU should be stable on a 0.1% level for the next 5 years. By regular cross-checks of the four lamps of the collective, the stability is further assured. However, sudden jumps in the irradiance (section 3.1.2) were also observed for lamps of the collective, increasing the standard uncertainty to 0.5%.

10. In reference 14, the IFU radiometer has two working standards at its disposal. One standard is used regularly to calibrate the instrument. The second standard is used to check the calibration of the first one at certain intervals. When deviations between both standards become clear, they are recalibrated. Furthermore, the illuminance of both standards is monitored regularly. With this quality control plan the uncertainty due to drifts of working standards is kept below 0.5%.

11. In reference 15, since the irradiance of 1000 W FEL reference standards and 100 W working standards differ by a factor of approximately 4 at their calibration distances, nonlinearities of the IFU radiometer (section 4.6) used to calibrate the 100 W lamps lead to a standard uncertainty of 0.3%.

12. In reference 16, small short-term drifts of the IFU radiometer during the transfer of calibration to the 100 W lamps lead to a standard uncertainty of 0.2%.

13. Reference 17, based on the considerations in section 3.1.1, concludes that the uncertainty in the calibration points of the four reference standards used in the collective is about 1.8%.

In addition to the 17 error sources described above, uncertainties in the radiometric calibration may arise from stray light and temperature variations in the calibration laboratory or ventilation of the lamps. For the

Table 3. Standard Uncertainties ($k = 1$) in Radiometric Calibration of the Mobile IFU Spectroradiometer

Ref.	Error Source	Uncertainty, %
1	interpolation of certificate	0.2
2	scaling of distance	0.3
3	reference point of entrance optics	0.2
4	influence of the quartz dome	0.2
5	area of receiver	0.1
6	distance alignment FEL lamp	0.1
7	distance alignment 100 W lamp	0.1
8	alignment of FEL lamp	0.1
9	alignment of 100 W lamp	0.1
10	alignment of entrance optics	0.1
11	lamp current FEL lamp	0.1
12	lamp current 100 W lamp	0.1
13	stability collective standard	0.5
14	stability working standard	0.5
15	linearity of spectroradiometer	0.3
16	drift of spectroradiometer	0.2
17	uncertainty of collective standard	1.8

The combined uncertainty of references 1-16 is 1.0%.

Table 4. Parameters to Quantify the Effect of the Cosine Error on Spectral Measurements of the IFU Radiometer for Wavelengths 300, 350, and 400 nm and for solar zenith angles (SZA) 30° and 60°

Parameter	SZA=30°			SZA=60°		
	300 nm	350 nm	400 nm	300 nm	350 nm	400 nm
$C(\lambda,\vartheta,\varphi)$	0.869	0.869	0.869	0.471	0.471	0.471
$q(\lambda)$	0.49	0.62	0.75	0.2	0.42	0.6
$D(\lambda)$	0.981	0.981	0.981	0.981	0.981	0.981
u_C	0.003	0.003	0.003	0.004	0.004	0.004
u_q	0.05	0.06	0.06	0.05	0.07	0.08
u_D	0.007	0.007	0.007	0.007	0.007	0.007
	$R_C(\lambda)$ and Its Uncertainty for Cloudless Sky					
$R_C(\lambda)$	0.992	0.995	0.998	0.973	0.965	0.958
$u_{R_C}(\lambda)$	0.004	0.004	0.003	0.006	0.006	0.006
$u_{R_C}(\lambda)\,/\,R_C(\lambda)$, %	0.4	0.4	0.3	0.6	0.6	0.6
	$R_C(\lambda)$ and Its Uncertainty for Cloudy Sky					
$R_C(\lambda)$	0.987	0.988	0.989	0.977	0.973	0.969
$u_{R_C}(\lambda)$	0.007	0.008	0.008	0.009	0.011	0.014
$u_{R_C}(\lambda)\,/\,R_C(\lambda)$, %	0.7	0.8	0.8	0.9	1.1	1.4

The parameter $R_C(\lambda)$ expresses the deviation of measurements with the IFU radiometer from the true irradiance due to the cosine error of this instrument. See text for additional parameter definitions. The aerosol optical depth $\tau(300)$ used for the calculation of $q(\lambda)$ was set as 0.1 ± 0.1. All uncertainties are based on a coverage factor of $k = 1$.

IFU radiometer these contributions have been reduced to an insignificant level.

The combined uncertainty of references 1 to 16, as calculated with (8), is 1.0%. Reference 17 is separated to demonstrate that the uncertainty of the reference standards exceeds the combined uncertainty of all other sources of error in the radiometric calibration.

4.2. Cosine Error

In section 3.2 the variable $R_C(\lambda)$ was introduced. It is the ratio of irradiance measured with a radiometer that is affected by a cosine error to the true irradiance. $R_C(\lambda)$ is calculated from the parameters $q(\lambda)$, $C(\lambda,\vartheta_{\text{Sun}},\varphi_{\text{Sun}})$, and $D(\lambda)$ according to (12). The standard uncertainty $u_{R_C}(\lambda)$ of $R_C(\lambda)$ is calculated with (13).

The cosine error of the entrance optics of the IFU radiometer is +0.3% at 30° incidence angle ($C(30°) = 0.869$) and −5.9% at 60° incidence angle ($C(60°) = 0.471$) [*Bernhard and Seckmeyer*, 1997]. The uncertainties of these values are caused mainly by misalignment of the equipment used to measure the angular response (section 3.2.1) and by a slight dependence of the error on the azimuth angle φ. The dependence of the error on wavelength is insignificant [*Bernhard and Seckmeyer*, 1997]. We find that the standard uncertainty u_C of $C(\vartheta)$ is 0.003 for $\vartheta = 30°$ and 0.004 for $\vartheta = 60°$. The relative uncertainty $u_C/C(\vartheta)$ is 0.3% for 30° and 0.8% for 60°.

In section 3.2 the variable $D(\lambda)$ was defined as the ratio of sky irradiance, measured by a radiometer with cosine error, to the true sky irradiance. If sky radiance is isotropic, $D(\lambda)$ could be replaced by $D_{\text{isotr}}(\lambda)$ as defined in (14). For the IFU radiometer, $D_{\text{isotr}}(\lambda)$ is 0.981, which means that isotropic sky irradiance is underestimated by 1.9%. On the basis of the considerations in section 3.2.3, the uncertainty u_D that is due to also using $D_{\text{isotr}}(\lambda)$ for a real clear sky with inhomogeneous radiance distribution is estimated to be 0.007 for the IFU instrument.

The third parameter needed to calculate $R_C(\lambda)$ and $u_{R_C}(\lambda)$ is the ratio of direct to global irradiance, $q(\lambda)$. For cloudless sky, $q(\lambda)$ depends mainly on SZA and aerosol optical depth τ; see Figure 1. For the uncertainty estimate presented here, τ is set to 0.1 ± 0.1. The corresponding ratio $q(\lambda)$ and its uncertainty u_q were calculated with the UVSPEC model.

The data from *Bernhard and Seckmeyer* [1997] suggest that, for days with scattered clouds, $R_C(\lambda)$ varies approximately between its value for clear sky and its value for overcast sky. This was only demonstrated for one particular day, however, and this finding therefore may not be true for all cloud situations. In the absence of additional data, we assume that a reasonable estimate of $R_C(\lambda)$ for cloudy skies is to set $R_C(\lambda)$ as the average of its values for clear and overcast sky. The uncertainty u_{R_C} of this estimate is calculated with (16): u_{R_C} is the sum of the uncertainty for clear sky and the uncertainty arising from the varying atmospheric conditions under cloudy skies.

In Table 4, $R_C(\lambda)$ and its uncertainty are presented for cloudless and cloudy skies as a function of wave-

length and SZA. For cloudless skies, $R_C(\lambda)$ varies between 0.958 and 0.99. Without cosine correction the measurements of the IFU radiometer would therefore be too low by as much as 4.2%. The uncertainty of the correction is about 0.4% for 30° SZA and 0.6% for 60° SZA. For cloudy skies the uncertainty u_{R_C} is about twice as large as for the clear-sky case. For all calculations above, an aerosol optical depth of 0.1 ± 0.1 was assumed. If no information about the aerosol is available, u_{R_C} becomes larger.

4.3. Spectral Resolution

The fine structure of the solar spectrum caused by the Fraunhofer lines is smoothed out considerably by the finite resolution of the IFU radiometer, see Figure 2: the ratio $R_R(\lambda, B)$ of measurements with the IFU instrument to the true global spectral irradiance $E_G(\lambda)$ may reach values of up to 14. However, if biologically weighted irradiance is derived from spectral measurements, the errors caused by the instrument's finite bandwidth are mainly a result of the slope of the solar spectrum in the UVB cutoff rather than the fine Fraunhofer structure.

The ratio $R_{R,\mathrm{Bio}}(B)$ of biologically weighted irradiance measured with the IFU radiometer to the true irradiance was calculated with (18). For SZAs of 30° and 60° the measurements of the IFU radiometer were found to be too high by 0.1% (erythemal irradiance) and 0.3% (DNA weighted irradiance). Compared with other sources of error, these systematic errors are negligible and are not routinely corrected.

Systematic errors in spectral irradiance caused by the resolution in combination with the steep increase of the solar spectrum in the UVB were quantified in section 3.3.2 by the fit functions $R_R^*(\lambda, B)$. For the bandwidth of the IFU radiometer, $R_R^*(\lambda, B)$ is 1.006 at 30° SZA, 320 DU, and 300 nm. At 60° SZA the ratio is 1.017. Systematic errors estimated with these fit functions neglect completely the influence of the Fraunhofer structure, but the functions provide useful information about the effect of the ozone cutoff on measured solar spectra.

4.4. Wavelength Misalignment

The wavelength uncertainty of the IFU radiometer is 0.04 nm if the calibration is checked on a weekly basis. This was determined from regular measurements of line spectra from low-pressure mercury lamps and correlation methods, where the Fraunhofer structure is used to determine wavelength shifts [*Slaper et al.*, 1995].

Uncertainties in biologically weighted irradiance due to wavelength shifts are calculated with (23). For the IFU radiometer the standard uncertainty in erythemal irradiance caused by the wavelength uncertainty of 0.04 nm is 0.7%; the respective uncertainty for DNA weighted irradiance is 1.4%. Both uncertainties depend only weakly on SZA and total ozone; see Table 2.

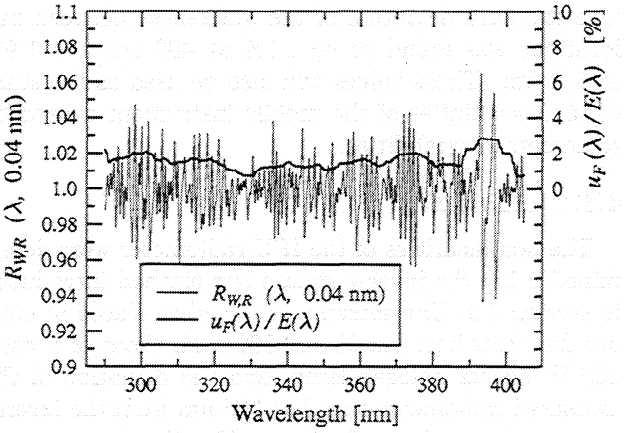

Figure 8. Uncertainty of the IFU radiometer, caused by wavelength shifts and the Sun's Fraunhofer lines. The thin line (left axis) is the ratio $R_{W,R}(\lambda, \Delta\lambda)$ of a model spectrum, which was deliberately shifted by 0.04 nm to longer wavelengths, to the unshifted spectrum. The applied wavelength shift of 0.04 nm is the wavelengh uncertainty of the IFU radiometer. The thick line (right axis) is the relative standard uncertainty $u_F/E(\lambda)$ caused by this wavelength shift according to (25).

As proposed in section 3.4.2, uncertainties in spectral measurements caused by wavelength shifts in combination with the Fraunhofer structure are quantified with the standard deviation σ_F, defined in (25). To study the influence of the Fraunhofer structure independently from the effect of the ozone cutoff, we modeled a spectrum by setting the model parameter "total ozone column" to 0, convolved the spectrum with the slit function of the IFU radiometer, shifted the spectrum by the wavelength uncertainty of the instrument (0.04 nm), and, finally, formed the ratio $R_{W,R}(\lambda, 0.04\ \mathrm{nm})$ of shifted and unshifted spectra. By applying (25), the uncertainty $u_F(\lambda)$ was determined. The result is shown in Figure 8. The relative uncertainty $u_F(\lambda)/E(\lambda)$ varies between 0.7% and 2.8%.

Systematic errors in spectral measurements caused by wavelength shifts in combination with the steep increase of the solar spectrum in the UVB were quantified in section 3.4.3 by the fit functions $R_{W,R}^*(\lambda, \Delta\lambda)$. For the wavelength uncertainty of the IFU radiometer the ozone cutoff leads to uncertainties in the measured irradiance at 300 nm of 2.1% (30° SZA, 320 DU) and 3.3% (60° SZA, 320 DU).

4.5. Radiometric Stability

The radiometric stability was determined from calibration data of the stationary IFU spectroradiometer. This is almost identical to the mobile instrument but, in contrast to the mobile instrument, is operated uninterrupted over long time periods. The stationary instrument is calibrated weekly. The difference of consecutive calibrations follows a normal distribution [*Mayer*, 1997].

The standard deviation of the differences between calibrations was found to be 1.1% at 400 nm and 1.9% at 300 nm. These values will also be used as the standard uncertainties of the mobile instrument caused by radiometric instabilities.

4.6. Nonlinearity

The nonlinearities of the IFU radiometer were determined using the inverse square law method introduced in section 3.6. The entrance optics were placed at various distances between 20 and 360 cm in front of a small 100 W quartz halogen lamp, and the deviation of the measured radiometer signal at 365 nm from the inverse square law was then calculated. The distance range allows nonlinearities to be determined over only about 2.5 orders of magnitude. To cover the whole dynamic range of the system, measurements were conducted at different light levels. With four overlapping measurement series the nonlinearity was determined over 7 orders of magnitude. The result is shown in Figure 9. The nonlinearity was measured separately for each amplifier stage of the system. The result for each stage is depicted with a different symbol. For signal levels between 10^3 and 10^7, deviations from linearity are smaller than $\pm 1\%$; the corresponding standard uncertainty is 0.6%. Nonlinearities affect both calibration and solar measurements. The combined uncertainty is therefore $\sqrt{2} \times 0.6\% = 0.8\%$.

Below a signal level of 10^3, the measurement becomes affected by noise. Especially for measurements in the most sensitive amplifier stage (below a level of 10^2), noise prevents a correct assessment of nonlinearities.

For signal levels above 10^7, the PMT current of the IFU radiometer is too high. The operation of the instrument is therefore restricted to levels below 10^7. The deviation from linearity of the IFU radiometer depends on its amplifier stage. Polynomial fit functions, which are usually applied to correct nonlinearities [*Kostkowski*, 1997], cannot correct for these features.

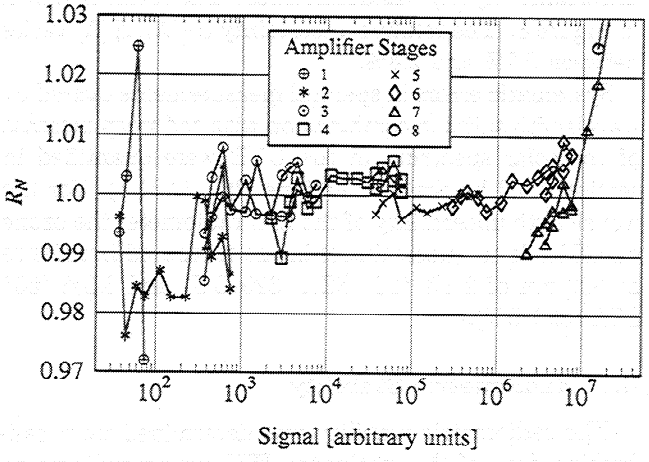

Figure 9. Nonlinearity of the mobile IFU spectroradiometer. The curves show the ratio $R_N(365\text{ nm}, S)$ of measurements of the IFU instrument to the true irradiance, which would be measured by a perfectly linear radiometer. R_N is displayed as a function of the signal S of the IFU radiometer. The different symbols refer to measurements at different amplifier stages (see legend).

4.7. Noise

The signal-to-noise ratio, of the IFU radiometer can be closely approximated by the function

$$\mathrm{S/N}\,[S(\lambda)] \;=\; 1.25\,\sqrt{S(\lambda)}, \qquad (35)$$

where $S(\lambda)$ is the signal of instrument in the units given by the radiometer's software. By combining (29) and (35), the standard uncertainty of the noise contribution, $u_N(\lambda)$, is calculated for the wavelengths 300, 350, and 400 nm and for solar zenith angles of 30° and 60°. The signal-to-noise contribution from the calibration, $\mathrm{S/N}[S_L(\lambda)]$, was scaled in (29) by a factor of $\sqrt{2}$, because a calibration of the IFU radiometer is based on the average of two calibration scans. For a solar zenith angle of 30° and wavelengths above 295 nm, $u_N(\lambda)$ is dominated by calibration noise. At smaller wavelengths, $u_N(\lambda)$ is mainly affected by the noise during the recording of a solar spectrum. The relative uncertainty $u_N(\lambda)/E_G(\lambda)$ varies between 4% (300 nm and 60° SZA) and 0.6% (400 nm and 30° SZA).

The uncertainty due to noise in biologically weighted irradiances, $u_{N_{\mathrm{Bio}}}$, was calculated with (31). The relative uncertainty $u_{N_{\mathrm{Bio}}}/E_{\mathrm{Bio}}$ is 0.3% for erythemal irradiance and 0.4% for DNA weighted irradiance.

The detection limit of the IFU radiometer is limited by noise. With (32) the noise equivalent irradiance of the instrument was found to be $\mathrm{NEI} = 7 \times 10^{-4}\ \mathrm{mW/(m^2\ nm)}$ for the instrument's bandwidth of 0.574 nm.

4.8. Stray Light

Stray light in the signal of the IFU radiometer is below the detection limit, and so no uncertainty arises from stray light.

4.9. Timing Errors

The system is equipped with a radio clock, and this keeps the time correct to within 1 s. Timing errors are therefore negligible.

4.10. Further Sources of Error of IFU Radiometer

Uncertainties due to the time constant of the lock-in amplifier are kept small by introducing a sufficiently large waiting time after setting a new wavelength. The remaining uncertainties are 0.5% in spectral irradiance and 0.2% in weighted integrals.

A small amount of hysteresis is present in the responsivity of the PMT. This is caused by the rapid change in signal when a new spectrum starts at low signal levels after the high signal levels prevailing at the end of the previous spectrum. This hysteresis leads to an uncertainty of 0.5%.

Table 5. Uncertainties of the Mobile IFU Spectroradiometer for Wavelengths 300, 350, and 400 nm and solar zenith angles (SZA) 30° and 60°

Ref.	Contribution	Relative Standard Uncertainty $u/E(\lambda)$, %									
		SZA=30°					SZA=60°				
		300 nm	350 nm	400 nm	Ery	DNA	300 nm	350 nm	400 nm	Ery	DNA
1	calibration	1.0	1.0	1.0	1.0	1.0	1.0	1.0	1.0	1.0	1.0
2	collective normal	1.8	1.8	1.8	1.8	1.8	1.8	1.8	1.8	1.8	1.8
3	cosine error	0.4	0.4	0.3	0.4	0.4	0.6	0.6	0.6	0.6	0.6
4	leveling	0.1	0.1	0.1	0.1	0.1	0.1	0.2	0.2	0.1	0.1
5	λ shift UVB	2.1	0.0	0.0	0.7	1.4	3.3	0.0	0.0	0.7	1.4
6	λ shift + Fraunh.	2.0	1.1	2.0	...	...	2.0	1.1	2.0	...	...
7	stability	1.9	1.5	1.1	1.8	1.8	1.9	1.5	1.1	1.8	1.8
8	nonlinearity	0.8	0.8	0.8	0.8	0.8	0.8	0.8	0.8	0.8	0.8
9	noise	2.6	1.0	0.6	0.3	0.4	4.0	1.0	0.6	0.3	0.4
10	lock-in	0.5	0.5	0.5	0.2	0.2	0.5	0.5	0.5	0.2	0.2
11	PMT hysteresis	0.5	0.5	0.5	0.5	0.5	0.5	0.5	0.5	0.5	0.5
Combined uncertainty		4.9	3.2	3.3	3.0	3.3	6.3	3.2	3.4	3.1	3.3
Expanded uncertainty		9.9	6.3	6.6	6.1	6.5	12.7	6.4	6.7	6.1	6.6

The uncertainties in erythemally weighted irradiance (Ery) and DNA weighted irradiance (DNA) are shown as well for both zenith angles. The uncertainties refer to measurements under cloudless sky with an aerosol optical depth of 0.1 and a ozone column of 320 DU. Calibrations are performed weekly. The two last rows give the combined and expanded ($k = 2$) uncertainties, calculated with Equation (8).

4.11. Combined uncertainty of the IFU radiometer

On the basis of the different contributions described in the last sections, the combined uncertainty of the IFU radiometer was calculated with (8). The result is shown in Table 5. The values refer to measurements under cloudless skies with an aerosol optical depth of 0.1 and an total ozone of 320 DU.

Reference 1 of Table 5 contains the uncertainties arising from the radiometric calibration as compiled in Table 3. The uncertainty in the calibration of the four reference standards of 1.8% is listed separately in reference 2. Reference 5 gives the uncertainties caused by the wavelength uncertainty of 0.04 nm in combination with the steep slope of the solar spectrum in the UVB. Reference 6 contains the uncertainties caused by the wavelength uncertainty in combination with the Fraunhofer structure of the solar spectrum. (The uncertainties in erythemally and DNA weighted irradiance due to the Fraunhofer structure are addressed in reference 5; see section 4.4). Reference 10 lists the uncertainties arising from the time constant of the lock-in amplifier.

For 30° SZA the expanded uncertainty (last row of Table 5) varies between 9.9% at 300 nm and 6.3% at 350 nm. For 60° SZA the expanded uncertainty at 300 nm is 12.7%. For longer wavelengths the uncertainty is almost independent of solar zenith angle. The expanded uncertainties in biologically weighted irradiances are 6.1% (erythema) and 6.6% (DNA).

5. Discussion and Conclusions

In section 3, all sources of error affecting measurements of global spectral irradiance were thoroughly introduced and methods were presented to quantify systematic errors and uncertainties depending on the characteristics of a spectroradiometer (e.g., its bandwidth and wavelength error). The methods and equations proposed are not restricted to a specific instrument but can be applied to most of the spectroradiometers currently deployed for UV research. With the help of model calculations the effects of different atmospheric conditions were included in the error analysis. Some errors are nearly independent of the state of the atmosphere. However, uncertainties arising from the cosine error depend significantly on the distribution of sky radiance and on the ratio $q(\lambda)$ between direct and global irradiance (section 3.2 and Table 4). Uncertainties at short wavelengths depend additionally on solar zenith angle and total ozone (Table 2). If clouds lead to a significant reduction of the irradiance, the uncertainties caused by noise are enhanced. Since the signal-to-noise ratio is dominated by the calibration, the influence of clouds on noise is significant only for UVB wavelengths or when the solar elevation is small.

Some uncertainty estimates (for example, the uncertainty in cosine correction factors under cloudy sky, $u_{K_C}^{\text{cloudy}}$) may themselves be the subject of uncertainties, because the underlying data set does not allow for appropriate statistics. Also in these cases, however, un-

certainty values are given. This is preferable to ignoring an error source completely.

On the basis of the general considerations in section 3, a complete uncertainty table of the mobile IFU spectroradiometer was established in section 4. One goal of this examination was to show how the methodologies developed in the first part can be applied to a real instrument. The uncertainties of the instrument are compiled in Table 5 for different wavelengths and solar zenith angles. The expanded uncertainty ($k = 2$) of measurements of global spectral irradiance conducted with the IFU radiometer vary between about 6.3% in the UVA and 12.7% at 300 nm and 60° solar zenith angle. The expanded uncertainties in biologically weighted irradiance are about 6.3%.

At 300 nm the most important sources of error are wavelength misalignment and noise. At longer wavelengths and in weighted integrals the calibration uncertainties of the reference standards used to determine the spectral responsivity of the instrument become most important. Here instabilities of the instrument also significantly reduce its accuracy.

Noise at short wavelengths originates from the solar measurement rather than from the calibration. This cannot be reduced without extending the scan time. A reduction of noise at longer wavelengths is possible, for example, by averaging over more than two calibration scans or by using 1000 W calibration working standards rather than 100 W lamps. However, this will not lead to a substantial improvement of the accuracy because noise contributes only little to the overall uncertainty in the UVA.

The wavelength uncertainty of 0.04 nm of the IFU radiometer is already rather good compared with similar instruments [*Bais*, 1998; *Seckmeyer et al.*, 1998]. This value of the uncertainty is valid if the wavelength alignment is checked weekly. If it is inspected daily (which is the case during specific campaigns), the wavelength uncertainty can be reduced further to 0.02 nm. Alternatively, an uncertainty of 0.02 nm can be reached by correlating the structure of the measured spectra with the respective structure in a reference solar spectrum [*Webb*, 1997]. At short wavelengths, however, where a small wavelength uncertainty is most important, the accuracy of such methods is limited owing to interference between structures in the ozone cross section and the Fraunhofer lines.

Although efforts have been made in the past to reduce the uncertainties of standard lamps disseminated by national standards laboratories [*Sperling et al.*, 1996], the lamps are still an important source of uncertainty. Our investigations have confirmed that these lamps may suffer from abrupt changes in their radiation output. We therefore suggest that standards laboratories further improve the calibration transfer, for example, by selecting lamps that are more stable or by establishing detector-based calibration standards for the UV.

The uncertainties caused by instabilities in the radiometric calibration were derived by evaluating the calibration record of the stationary IFU radiometer. This procedure is justified because both the stationary and the mobile system have similar configurations. However, the mobile instrument is mainly deployed in campaigns where the calibration is often checked on a daily basis. Under these circumstances, uncertainties arising from radiometric instabilities can be reduced to 0.5%.

Intercomparison campaigns in the past have shown that the cosine error is one of the most important sources of uncertainty [*Webb*, 1997; *Bais*, 1998]. The systematic errors arising from the cosine error of the IFU radiometer are corrected routinely. Correcting factors range between 1.00 and 1.05. The remaining uncertainties after the application of the correction algorithm are below 0.6% for cloudless sky and below 1.4% for cloudy skies. This small contribution of the cosine error to the overall uncertainty of the IFU radiometer can be attributed to the good characteristics of the newly developed entrance optics [*Bernhard and Seckmeyer*, 1997].

Spectra measured with finite bandwidth instruments overestimate the value of broadband irradiances. For the IFU radiometer the corresponding systematic error of this effect is only 0.1% for erythemal irradiance and 0.3% for DNA weighted irradiance. At 300 nm and 60° SZA the error is 1.7%. Though these errors are small, they depend quadratically on bandwidth and will therefore be substantial for an instrument with a broad slit function. These errors are neglected if spectral measurements are normalized to a common bandwidth, e.g., by deconvolution techniques [*Slaper et al.*, 1995].

The uncertainty of the IFU radiometer may be compared with some uncertainty estimates published elsewhere. *Bener* [1960] used a prism double monochromator to measure solar UV radiation and conducted an uncertainty analysis of similar detail to that performed in this paper. At 300 nm and 40° SZA he reports a 2σ uncertainty of 13% for his instrument; at 60° zenith angle the uncertainty is 17%. These values are comparable to the expanded uncertainties of the IFU radiometer.

A further substantial examination of uncertainties in solar measurements is presented by *Kostkowski* [1997]. The instrument described herein is designed for direct rather than global irradiance measurements and was only deployed for 1 day. The uncertainties given by *Kostkowski* [1997] arising from noise, radiometric instabilities, and the entrance optics are therefore much smaller than in our case. The expanded uncertainty reported is 3.2% at 295 nm and 7° SZA. However, if we (1) base our uncertainty estimate on the optimal operation conditions during campaigns (wavelength uncertainty 0.02 nm, uncertainty due to instabilities 0.5%); (2) set the uncertainty of the reference standards to 0.8% as it is done by *Kostkowski* [1997]; (3) reduce the noise level by a factor of $\sqrt{10}$, which takes into account the differ-

ence in throughput of global and direct optics; and (4) neglect the uncertainties introduced by the cosine error, the expanded uncertainty of our radiometer becomes 4.3% at 300 nm and 30° SZA. This uncertainty is nearly the same as the uncertainty of the instrument described by *Kostkowski* [1997]. This example demonstrates that great care must be taken if uncertainty specifications of two instruments are compared: it is meaningless to give a combined uncertainty without an explanation of its derivation.

The desired uncertainty of a radiometer depends on the intended use of its data. For trend detection, in particular, a low uncertainty is required. For example, for UV spectroradiometers deployed in the Network for the Detection of Stratospheric Change (NDSC) the uncertainty should be small enough for a long-term change in UV resulting from a 1% change in ozone to be detected [*McKenzie et al.*, 1997]. The authors conclude that this goal can be reached only if the overall calibration uncertainty of NDSC spectroradiometers is less than ±5%, their detection threshold is of the order of 10^{-6} W/(m^2 nm), and the wavelength uncertainty is less than ±0.05 nm. Though the mobile IFU spectroradiometer meets these requirements, the ultimate goal of the NDSC, namely, detecting a 1% ozone change in UV data, is still difficult to achieve.

In Figure 10 the percentage change in global spectral irradiance caused by a 1% and a 3% change of total ozone is compared with the expanded ($k = 2$) uncertainty of the IFU radiometer. Three scenarios are considered. The uncertainties of scenario A are the same as presented in Table 5 (30° SZA, wavelength uncertainty 0.04 nm, weekly calibrations). For scenario B the wavelength uncertainty was reduced to 0.02 nm because this uncertainty can be reached by postprocessing of the data. Additionally, the uncertainty of the reference standard was set to 0 because the absolute scale is not important to detect relative trends. Scenario C is based on the same assumptions as scenario B. In addition, the uncertainty introduced by noise is set to 0 because the influence of noise in individual spectra averages out partly if long-term series are analyzed. This assumption is not applicable near the detection limit, however. The relative uncertainty of scenario C near the detection limit is parameterized by NEI/$E(\lambda)$, where the noise equivalent irradiance (NEI) is set to 7×10^{-4} mW/(m^2 nm). Thus scenario C is the lower limit of the uncertainty relevant for the detection of trends over sufficiently large time periods.

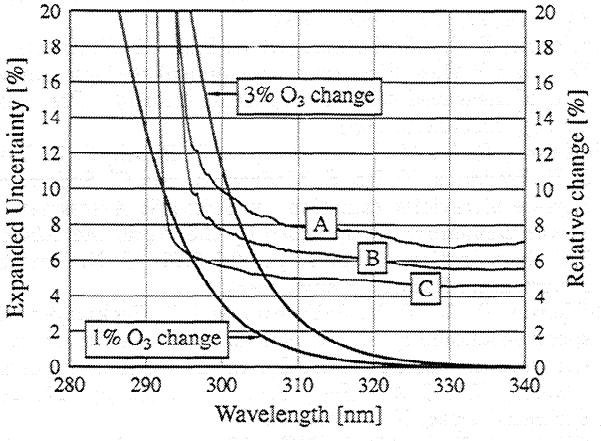

Figure 10. Percentage change in global spectral irradiance caused by a 1% and 3% change of total ozone compared with the expanded ($k = 2$) uncertainty of the IFU radiometer. The change in irradiance was calculated for 30° solar zenith angle and 300 DU (right axis). The uncertainty of the instrument (left axis) is given for the three scenarios A, B, and C described in the text.

Figure 10 shows that for all three scenarios a change in UV due to a 1% change in ozone cannot be detected: the expanded uncertainties are higher than the relative change in UV (except scenario A at 293 nm). However, the consequences of a 3% change in ozone should be detectable by all scenarios by analyzing the change in UV below 300 nm.

Ozone-related midlatitude trends in UV are expected to be only a few percent per decade [*McKenzie et al.*, 1994]. Figure 10 indicates that trends of this magnitude have only a possibility of being detected with spectroradiometers. Broadband UV instruments (e.g., Robertson-Berger meters) are not sensitive enough at wavelengths below 300 nm, which are affected mostly by ozone changes.

The uncertainty of an instrument is not the only parameter to judge whether trend detection is possible or not. Other important parameters are the time span of available data; the natural variability of UV radiation, which masks trends efficiently; and the autocorrelation of noise in the data [*Weatherhead et al.*, 1998]. Work still needs to be done to determine the magnitude of trends that can be unambiguosly detected with current instrumentation. A thorough uncertainty estimate forms the basis for such a work.

Acknowledgments. NSO/Kitt Peak FTS data used here were produced by NSF/NOAO. We thank M. VanHoosier and his team from the Naval Research Laboratory, Washington D.C., for making the SUSIM/ATLAS 3 spectrum available. In particular, we wish to express our thanks to Bernhard Mayer and Timothy Martin for their valuable comments to the manuscript, and to Biospherical Instruments Inc. for support in finalizing the publication. This work was funded by the German Ministry of Science, Education, Research and Technology and by the Commission of the European Community, contract ENV4-CT95-0177 (SUVDAMA).

References

Bais, A. F., C. S. Zerefos, and C. T. McElroy, Solar UVB measurements with the double- and single-monochromator Brewer Ozone Spectrophotometer, *Geophys. Res. Lett.*, *23*(8), 833-836, 1996.

Bais, A. F., Spectroradiometers: Operational errors and

uncertainties, in *Solar Ultraviolet Radiation: Modelling, Measurements and Effects, NATO ASI Ser., Ser. I*, vol. 52, edited by C. S. Zerefos and A. F. Bais, pp. 165-173, Springer-Verlag, New York, 1997.

Bais, A. F. (Ed.), Standardization of ultraviolet spectroradiometry in preparation of a European network (SUSPEN), final report, Eur. Comm., Dir. Gen. XII, Luxembourg, 1998.

Bais, A. F., S. Kazadzis, D. Balis, C. S. Zerefos, and M. Blumthaler, Correcting global solar ultraviolet spectra recorded by a Brewer spectroradiometer for its angular response error, *Appl. Opt.*, *37*(27) 6339-6344, 1998.

Bener, P., Investigation on the spectral intensity of ultraviolet sky and sun+sky radiation (between 297.5 mμ and 370 mμ) under different conditions of cloudless weather at 1590 m a.s.l., *Tech. Summary Rep. 1, Contract AF 61(052)-54*, Phys.-Meteorol. Obs. Davos, Davos-Platz, Switzerland, 1960.

Bernhard, G., *Die Genauigkeit von Messungen der solaren UV-Globalbestrahlungsstärke bei verschiedenen Atmosphärenbedingungen*, 170 pp., Shaker, Frankfurt am Main, Germany, 1997.

Bernhard, G., and G. Seckmeyer, New entrance optics for solar spectral UV measurements, *Photochem. Photobiol.*, *65*(6), 923-930, 1997.

Bernhard, G., A. Moise, B. Mayer, and G. Seckmeyer, Measurements of spectral solar UV irradiance in tropical Australia, *J. Geophys. Res.*, *102*(D7), 8719-8730, 1997.

Bernhard, G., R. L. McKenzie, G. Seckmeyer, and P. V. Johnston, Ratio spectra as a quality control tool for solar spectral UV measurements, *J. Geophys. Res.*, *103*(22), 28,855-28,861, 1998.

Booth, C. R., T. B. Lucas, J. H. Morrow, C. S. Weiler, and P. A. Penhale, The United States National Science Foundation's polar network for monitoring ultraviolet radiation, in *Ultraviolet Radiation in Antarctica: Measurements and Biological Effects, Antarct. Res. Ser.*, edited by C. S. Weiler and P. A. Penhale, vol. 62, 17-37, AGU, Washington, D.C., 1994.

Brewer, A. W., A replacement for the Dobson Spectrophotometer?, *Pure Appl. Geophys.*, *106-108*, 919-927, 1973.

Commission Internationale de l'Éclairage (Ed.), The spectroradiometric measurements of light sources, *Publ. CIE 63*(TC-1.2), Paris, 1984.

Coulson, K. L., *Polarization and Intensity of Light in the Atmosphere*, A. Deepak, Hampton, Va., 1988.

Dahlback, A., and K. Stamnes, A new spherical model for computing the radiation field available for photolysis and heating at twilight, *Planet. Space Sci.*, *39*, 671-683, 1991.

Feister, U., R. Grewe, and K. Gericke, A method for correction of cosine errors in measurements of spectral UV irradiance, *Sol. Energy*, *60*(6), 313-332, 1997.

Gardiner, B. G., and P. J. Kirsch (Eds.), Setting standards for European ultraviolet spectroradiometers, *Air Pollut. Res. Rep. 53*, 138 pp., Off. for Off. Publ. of the Eur. Communities, Luxembourg, 1995.

Grant, R. H., and G. M. Heisler, Obscured overcast sky radiance distributions for ultraviolet and photosynthetically active radiation, *J. Appl. Meteorol.*, *36*, 1336-1345, 1997.

Gröbner, J., M. Blumthaler, and W. Ambach, Experimental investigation of spectral global irradiance measurement errors due to a non ideal cosine response, *Geophys. Res. Lett.*, *23*(18), 2493-2496, 1996.

Harris, N. R. P., et al., Ozone measurements, in *Scientific Assessment of Ozone Depletion: 1994*, edited by the World Meteorological Organization, chap. 1, pp. 1.1-1.54, U. N. Environ. Programme, Nairobi, Kenya, 1994.

Huber, M., M. Blumthaler, and W. Ambach, A method for determining the wavelength shift for measurements of solar UV-radiation, in *Atmopheric Radiation, Proc. SPIE Int. Soc. Opt. Eng.*, *2049*, 354-357, 1993.

International Standards Organization (ISO), *Guide to the Expression of Uncertainty in Measurement*, Geneva, 1993.

Kaye, J. A., and T. L. Miller, The ATLAS series of shuttle missions, *Geophys. Res. Lett.*, *23*(17), 2285-2288, 1996.

Kjeldstad, B., B. Johnsen, and T. Koskela (Eds.), The nordic intercomparison of ultraviolet and total ozone instruments at Izaña, October 1996, final report, *Meteorol. Publ. 36*, Finn. Meteorol. Inst. Helsinki, 1997.

Köhler, U., W. Vandersee, and P. Winkler, Spektrale und integrale Messungen der UV-B-Strahlung im Vergleich zu Ozonmessungen, *Abschlußber. BayFORKLIM-Proj. B I 10*, Dtsch. Wetterdienst, Meteorol. Obs., Hohenpeißenberg, Germany, 1995.

Kostkowski, H. J., *Reliable Spectroradiometry*, 609 pp., Spectroradiometry Consult., La Plata, Md., 1997.

Krochmann, J., Über Ermüdungsmessungen an Photovervielfachern, *Lichttechnik*, *5/1963*, 266-268, 1963.

Kurucz, R. L., I. Furenlid, J. Brault, and L. Testerman, Solar flux atlas from 296 to 1300 nm, in *National Solar Observatory Atlas 1*, Harvard Univ. Press, Cambridge, Mass., 1984.

Lide, D. R. (Ed.), *Handbook of Chemistry and Physics*, CRC Press, Boca Raton, Fla., 1990.

Liu, Y., and K. Voss, Polarized radiance distribution measurement of skylight, II, Experiment and data, *Appl. Optics*, *36*(33), 8753-8764, 1997.

Mayer, B., A. Kylling, and G. Seckmeyer, Systematic long-term comparison of spectral UV measurements and UVSPEC modeling results, *J. Geophys. Res.*, *102*(D7), 8755-8767, 1997.

Mayer, B., *Messung und Modellierung der spektralen UV-Bestrahlungsstärke in Garmisch-Partenkirchen*, 135 pp., Wiss-.Verl. Maraun, Frankfurt am Main, Germany, 1997.

Mayer, B., A. Kylling, S. Madronich, and G. Seckmeyer, Enhanced absorption of UV irradiance due to multiple scattering in clouds: Experimental evidence and theoretical explanation, *J. Geophys. Res.*, *103*(D23), 31,241-31,254, 1998.

McKenzie, R. L., P. V. Johnston, M. Kotkamp, and A. Bittar, Solar ultraviolet spectroradiometry in New Zealand: Instrumentation and sample results from 1990, *Appl. Opt.*, *31*(30), 6501-6509, 1992.

McKenzie, R. L., G. Seckmeyer, C. Roy, M. Kotkamp, R. Erb, and P. Gies, First southern hemisphere intercomparison of measured solar UV spectra, *Geophys. Res. Lett.*, *20*(20), 2223-2226, 1993.

McKenzie, R. L., M. Blumthaler, C. R. Booth, S. B. Diaz, J. E. Frederick, T. Ito, S. Madronich, and G. Seckmeyer, Surface ultraviolet radiation, in *Scientific Assessment of Ozone Depletion: 1994*, edited by the World Meteorological Organization, chap. 9, pp. 9.1-9.22, U. N. Environ. Programme, Nairobi, Kenya, 1994.

McKenzie, R. L., P. V. Johnston, and G. Seckmeyer, UV spectro-radiometry in the network for the detection of stratospheric change (NDSC), in *Global Environmental Change, NATO ASI Ser., Ser. I*, vol. 52, pp. 279-287, Springer-Verlag, New York, 1997.

McKinlay, A. F., and B. L. Diffey (Eds.), A reference action spectrum for ultraviolet induced erythema in human skin, *CIE J.*, *6*(1), 17-22, 1987.

Moore, C. E. (Ed.), *The Solar Spectrum 2935Å to 8770Å, Second Revision of Rowland's Preliminary Table of Solar Spectrum Wavelengths, Natl. Bur. of Stand. Monogr. 61*, U. S. Dep. of Commer., Washington, D.C., 1966.

Sanders, C. L., Accurate measurements of and corrections for nonlinearities in radiometers, *J. Res. Natl. Bur. Stand. Sect. A, Phys. Chem.*, *76A*(5), 437-453, 1972.

Saunders, R. D., and J. B. Shumaker, Automated radiometric linearity tester, *Appl. Opt., 23*(20), 3504-3506, 1984.

Seckmeyer, G., and G. Bernhard, Cosine error correction of spectral UV irradiances, in *Atmospheric Radiation, Proc. SPIE Int. Soc. Opt. Eng., 2049*, 140-151, 1993.

Seckmeyer, G., G. Bernhard, B. Mayer, and R. Erb, High accuracy spectroradiometry of solar ultraviolet radiation, *Metrologia, 32*(6), 697-700, 1996.

Seckmeyer, G., B. Mayer, and G. Bernhard, *The 1997 Status of Solar UV Spectroradiometry in Germany: Results from the National Intercomparison of Spectroradiometers, Garmisch-Partenkirchen, August 1997,* 169 pp., Shaker, Aachen, Germany, 1998.

Setlow, R. B., The wavelengths in sunlight effective in producing skin cancer: A theoretical analysis, *Proc. Natl. Acad. Sci. U.S.A., 71*(9), 3363-3366, 1974.

Slaper, H., H. A. J. M. Reinen, M. Blumthaler, M. Huber, and F. Kuik, Comparing ground-level spectrally resolved solar UV measurements using various instruments: A technique resolving effect of wavelength shift and slit width, *Geophys. Res. Lett., 22*(20), 2721-2724, 1995.

Sperfeld, P., K.-H. Raatz, B. Nawo, W. Möller, and J. Metzdorf, Spectral-irradiance scale based on radiometric blackbody temperature measurements, *Metrologia, 32*(6), 435-439, 1996.

Sperling, A., S. Winter, K.-H. Raatz, and J. Metzdorf, Entwicklung von Normallampen für das UV-B-Meßprogramm, *PTB-Ber. PTB-Opt-52,* Braunschweig, Germany, 1996.

Thompson, A., et al., The 1994 North American interagency intercomparison of ultraviolet monitoring spectroradiometers, *J. Res. Natl. Inst. Stand. Technol., 102*(3), 1-43, 1997.

Voss, K. J., and Y. Liu, Polarized radiance distribution measurements of skylight, I, System description and characterization, *Appl. Opt., 36*(24), 6083-6094, 1997.

Walker, J. H., R. D. Saunders, J. K. Jackson, and D. A. McSparron, Spectral irradiance calibrations, *NBS Spec. Publ. U.S., 250-20*, 1987.

Walker, J. H., R. D. Saunders, J. K. Jackson, and K. D. Mielinz, Results of a CCPR intercomparison of spectral irradiance measurements by national laboratories, *J. Res. Natl. Inst. Stand. Technol., 96,* 647-668, 1991.

Weatherhead, E. C., et al., Factors affecting the detection of trends: Statistical considerations and applications to environmental data, *J. Geophys. Res., 103*(D14), 17,149-17,161, 1998.

Webb, A. R. (Ed.), Advances in solar ultraviolet spectroradiometry, *Air pollut. Res. Rep. 63*, 238 pp., Off. for Off. Publ. of the Eur. Communities, Luxembourg, 1997.

Webb, A. R., B. G. Gardiner, M. Blumthaler, P. Forster, M. Huber, and P. J. Kirsch, A laboratory investigation of two ultraviolet spectroradiometers, *Photochem. Photobiol., 60*(1), 84-90, 1994.

Webb, A. R., B. G. Gardiner, T. J. Martin, K. Leszczynski, J. Metzdorf, V. A. Mohnen, and B. Forgan, Guidelines for site quality control of UV monitoring, *Rep. Ser. 126*, Environ. Pollut. Monit. and Res. Programme, World Meteorol. Organ., Geneva, 1998.

Zeng, J., R. L. McKenzie, K. Stamnes, M. Wineland, and J. Rosen, Measured UV spectra compared with discrete ordinate method simulations, *J. Geophys. Res., 99*(D11), 23,019-23,030, 1994.

G. Bernhard, Biospherical Instruments Inc., 5340 Riley Street, San Diego, CA 92110-2621. (bernhard@biospherical.com)

G. Seckmeyer, Fraunhofer Institute for Atmospheric Environmental Research, Kreuzeckbahnstr. 19, D-82467 Garmisch-Partenkirchen, Germany. (seckmeyer@ifu.fhg.de)

(Received October 15, 1998; revised March 3, 1999; accepted March 5, 1999.)